Sound Synthesis of a Colombian Gaita by Means of Physical Modeling

Camilo Andrés Gómez Bonilla

Music Technology Area, Department of Music Research
Schulich School of Music
McGill University
Montreal, Canada

June 2020

2020/06/11

Abstract

Physical modeling of musical instruments has been a growing field of research since the early 1980s. At the time, the computational costs of physical models did not allow for real-time sound synthesis. Today, computational costs for real-time synthesis are not very prohibitive, and it is possible to implement more complex models with enough efficiency for real-time synthesis. Digital waveguides provide an efficient way of modeling one-dimensional wave propagation and implementing such physical models for sound synthesis.

While physical models of well-known instruments are ubiquitous in the literature, models of some lesser known traditional instruments from different cultures around the world are not. This thesis aims to provide a model of one of such instruments, the Colombian *gaita*. In this thesis, the acoustic response of a pair of gaitas was studied and a basic physical model of a gaita was developed and implemented for real-time synthesis using digital waveguide techniques found in the literature.

In order to determine if a cylindrical model would be an accurate representation for the instrument, impedance measurements were made on a pair of gaitas after their heads were removed. These measurements were then compared with the theoretical input impedance and reflection function results obtained using a transfer matrix model with the physical dimensions of a gaita. The results show the cylindrical approximation to be reasonable. While the results showed a similar frequency response and reflection function, they also showed some discrepancies in the amplitude of harmonic peaks, and the end reflection of some open hole configurations of the model.

The digital waveguide model was developed and implemented in MATLAB in order to compare its response with the measurements and theoretical results. The reflection function comparison showed, as expected, some discrepancies between the model and the measurements, particularly in the end reflection of certain open tonehole configurations. The model was then implemented for real-time sound synthesis with a graphical user interface using the JUCE framework and the Synthesis ToolKit. A time- and frequency-domain comparison of the sound synthesized by the model and recordings of the instrument show that while the model conveys the basic attributes of the sound of the instrument, it fails to accurately capture some other sonic qualities that are characteristic of the instrument. The most prominent differences between the model and the real instrument sounds are found to be the magnitudes of the higher-frequency harmonics and the overall noise content.

Sommaire

La modèlisation physique des instruments de musique est un domaine de recherche en croissance depuis le début des années 1980. Á l'époque, les coûts de calcul ne permettaient pas la synthèse de son en temps réel. Aujourd'hui, les coûts de calcul pour la synthèse en temps réel ne sont pas trop prohibitifs,il est même possible d'implanter des modèles plus complexes avec assez d'efficacité. Les guides d'ondes numériques constituent un moyen efficace pour modéliser la propagation des ondes unidimensionelles ainsi que la mise en œuvre de tels modèles physiques pour la synthèse de son.

Tandis que les modèles physiques des instruments bien connus sont omniprésents dans la littérature, les modèles de certains instruments traditionelles moins connus provenant de différentes cultures à travers le monde ne le sont pas. Cette thèse vise à proposer un modèle pour l'un de ces instruments, la *gaita* colombienne. Dans cette thèse, la réponse acoustique d'une paire de gaitas a été étudiée et un modèle physique élémentaire d'une gaita a été développé et mis en œuvre en utilisant les techniques des guides d'ondes numériques que l'on trouve dans la littérature.

Afin de déterminer si un modèle cylindrique serait une représentation adéquate pour cet instrument, des mesures d'impédance ont été effectuées sur une paire de gaitas après que leurs têtes aient été enlevées. Ces mesures ont ensuite été comparées avec les résultats de l'impédance d'entrée et la fonction de réflexion théoriques obtenus en utilisant un modèle de matrice de transfert avec les dimensions physiques d'une gaita. Les résultats montrent que l'approximation cylindrique est raisonnable. Si les résultats ont montré une réponse de fréquence et une fonction de réflexion similaires, ils ont également montré quelques écarts dans l'amplitude des pics harmoniques, ainsi que le reflet de la fin de l'instrument dans certaines configurations avec les trous de ton ouverts.

Le modèle de guides d'ondes numériques a été développé et mis en œuvre dans MATLAB afin de comparer la réponse avec les mesures et les résultats théoriques. La comparaison de la fonction de réflexion a montré, comme prévu, des écarts entre le modèle et les mesures, particulièrement dans les configurations avec les trous de ton ouverts. Le modèle a ensuite été mis en œuvre pour la synthèse en temps réel avec une interface graphique en utilisant le cadre logiciel JUCE et le Synthesis ToolKit. Une comparaison temps-fréquence du son synthètisé et des enregistrements de l'instrument montre que le modèle, bien qu'il transmet les attributs de base de l'instrument, ne parvient pas à capturer avec précision

certaines autres qualités sonores qui sont caractéristiques de l'instrument. Les différences les plus importantes entre le son du modèle et le son de l'instrument sont les amplitudes des harmoniques de haute fréquence et le contenu global du bruit.

Acknowledgments

I would like to extend my deep gratitude to my supervisor, Dr. Gary Scavone, for his support and guidance since the beginning of the project. I very much appreciate his patience and understanding during every step of the way. I would also like to thank Dr. Esteban Maestre, for checking in on my progress and being willing to offer help and guidance when I needed it. I am also very grateful to my Music Tech lab mates and colleagues, in particular Mathias Bredholt for his help using JUCE, Song Wang, for his help printing adaptors for the measurements and Harish Venkatesan for his endless encouragement and reassurance.

I have met many truly wonderful people and made a lot of good friends these past years in Montreal, and I feel very lucky and grateful to have crossed paths with them. In particular, I would like to thank my best friend, Silvana, and my partner, Trycia, for their unconditional support and encouragement on a daily basis, for constantly checking in on my progress, for being there for me when I needed anything, for being available to listen, for all the laughs, and for being my family and making me feel at home in Montreal.

Lastly, I will forever be grateful to my family: my dad, mom and sister, for their never ending support, encouragement and love. Without them I would not have been able to move to Montreal, let alone pursue my studies. They have never failed at providing the perfect amount of tough love to push me to do the best I can.

Contents

List of Figures

List of Tables

Chapter 1

Introduction

1.1 Motivation

Wind instruments are arguably the oldest pitched instruments in human history. Bone whistles and flutes survive from paleolithic sites dated to 40,000 BC, or even earlier. The simplest end-blown flute is a tube with an open end, for example a piece of bamboo [14]. The Colombian *gaita* is one of such instruments, and it is of great cultural importance along the Caribbean coast of the country.

Despite their cultural importance, the construction and playing of gaitas has historically been, and largely remains an oral tradition. In 2013, Ochoa [1] published a musicological study centered around this instrument. This study included topics such as the history of the instrument, basic aspects of the construction of the instrument, playing technique, and transcriptions of traditional gaita tunes. An acoustic study of the instrument was presented in 2002 by Juan Hernandez at the Pontificia Universidad Javeriana in Bogotá, Colombia, but it is currently unavailable to the public, and it did not concern the development of a physical model [15, 16].

Flute-like instruments have a superficially simple mechanism for sound production, yet the physics behind it, in particular, their excitation mechanism, can be quite complex. There has been extensive theoretical and experimental research conducted on flute-like instruments, including analyses of the air jet mechanism [17, 18, 19], and the behavior and characterization of the acoustic tube including the influence of toneholes, [20, 21, 22, 23, 24]. Modeling the behavior of these instruments and their underlying structures is a useful tool for understanding the sound production mechanisms and their complexities.

Time-domain modeling of acoustic structures has been a growing field of research in musical acoustics since the publication of the landmark paper by McIntyre et al [4]. Digital waveguide modeling is a technique for simulating one dimensional wave propagation in discrete-time, providing an efficient way of modeling strings and acoustic tubes using delay lines. These techniques have been documented by Smith [25, 26] and Välimäki [27], among others. The implementation of physical models of wind instruments using digital waveguides has also been widely researched, and some models can be found in the literature with varying degrees of complexity, such as the *SlideFlute* by Cook [28], models by Välimäki [29, 30], which also approached the issues of radiation and influence of toneholes, the saxophone model by Scavone [7], which refined the tonehole model and discussed the implementation of register holes, and the model by Verge [12], which approached the issue of the air jet mechanism in more detail. A model of a gaita hembra was presented in [13] using digital waveguide techniques, based on a recorder model by Välimäki. The parameters of said model were derived from a frequency-domain comparison between recordings of a real gaita and the output of the model.

The goal of this project is to implement a model of a Colombian gaita or *kuisi* based on the physical properties of the instrument, using the aforementioned techniques, and synthesize its sound in real time.

1.2 Thesis Overview

Chapter 2 presents an overview of Colombian gaitas, including their tuning, playing positions, and commonly used range. This chapter also reviews some acoustical principles of wind instruments that will be useful in the sections to follow, including the characterization of air columns, which are later used to compare the response of the instrument with both the theoretical and digital waveguide models. Chapter 3 presents an explanation of the physical modeling techniques used for the implementation of the model. It explains individual components that will be used to put the model together, including the modeling of the acoustic tube, toneholes and excitation mechanism of the model. Chapter 4 presents a comparison of the results obtained by measuring the impedance response of a pair of gaitas after their heads were taken off, with the theoretical results obtained using a transfer matrix model and the physical measurements of the instruments. Chapter 5 gives an overview of the implementation of the model. A comparison of the response of

the waveguide model with the measurements and the theoretical results presented in the previous chapter is made. It concludes with a comparison of the sound synthesized by the model and recordings of the instrument using a spectrogram and their frequency spectrum.

Chapter 2

Background

2.1 The Colombian *Gaita*

Gaitas are a traditional instrument from the Montes de María region of Colombia, near the Caribbean coast, and they are of great importance in the folklore and musical tradition of the region. A gaita is a wind instrument of indigenous origins consisting of an open-ended quasi cylindrical bore made of dry cactus (known as cardón). The mouthpiece, shown in Fig. 2.1 is made of a mixture of beeswax and coal [1], which is heated and attached to the tube. Figure 2.2 shows the tubes of the gaitas after their heads were removed and one of the heads next to them. Air is blown into the instrument through a small *feather*, originally made from a duck or turkey's feather, but more recently made of plastic attached to the wax/coal mixture. The angle and distance of the feather to the edge of the tube varies by instrument, and is usually set by trial and error. Gaitas are made in pairs: a macho (male) that has two holes, and a hembra (female) that has five holes. Neither the length of the tubes, which can vary between 75 and 85 cm, nor the sizes of the holes, which are usually close to 3/8 in, are standardized. The length of the tube has traditionally been dictated by the arm length of the intended player. Traditionally, the distance between the instrument's holes has been measured using the builder's fingers as a reference: 4 or 5 fingers from the end of the instrument to the lowest hole, and about 3 fingers between holes [1]. Gaitas are flute-like instruments, having a sound producing mechanisms similar to that of a recorder. These types of instruments consist of a linear system, an acoustic resonator, coupled to a non-linear excitation mechanism, an air-jet striking a sharp edge [31].
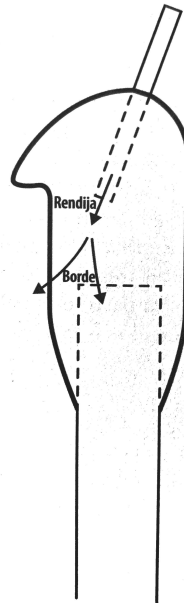
Fig. 2.1   Head of a gaita (from [1]).

Fig. 2.2   Tubes of gaitas after their heads were removed, next to one of the heads

2.1.1 Range and Tuning

A typical ensemble consists of 3 drums (*tambor alegre, tambor llamador* and *tambora*, a maraca, a gaita hembra and a gaita macho). Being artisanal, hand-made instruments, the tuning of gaitas has not been standardized. The lowest note of the instrument is usually somewhere near G♭2 and G2 [1]. Figure 2.3 illustrates the finger positions for a gaita hembra. Not shown in the diagram is position 0, with all of the toneholes closed, which will be considered for the measurements in this study. The fundamental notes are quite challenging to play, as they require a very soft blow pressure and they are not used very often [1]. Higher partials can be achieved by overblowing. Figure 2.4 shows an approximation of the common playing range of a gaita hembra. The two lowest notes shown on the left correspond to the fundamentals of positions 3 and 5, respectively, which are the only fundamentals commonly used in this instrument [1].
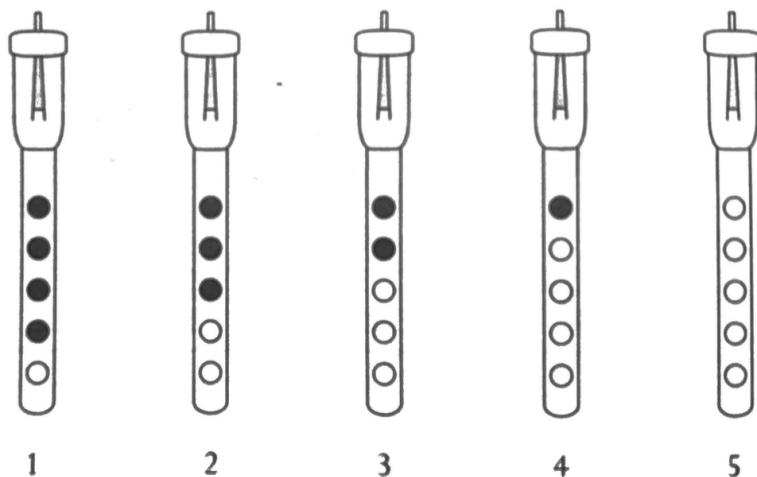
Fig. 2.3 Finger positions of a gaita hembra (from [1]). (Closed toneholes are shown in black)

Traditional gaitas do not play this exact set of notes. This is rather an approximation, quite close for all positions except for position two. In position 2, the fundamental note varies among instruments between a B♭ and a B. This ambiguity makes the tuning of the instrument vary between what would be a Western dorian and phrygian scales from position one.

Fig. 2.4 Approximation of the range of a gaita hembra (from [1]).

The gaita macho has 3 finger positions, as shown in Fig. 2.5. In a gaita macho, position 2 also varies in tuning, and the fundamental can be closer to a B♭, depending on the particular instrument.
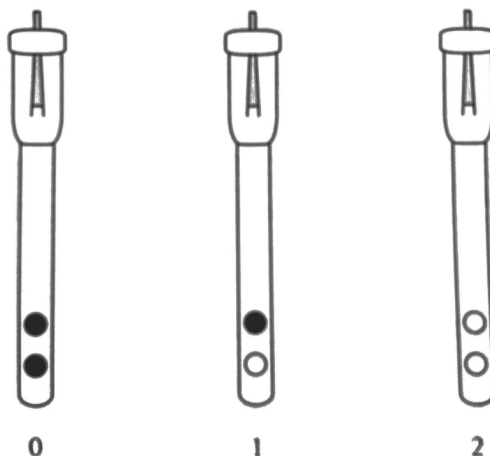
Fig. 2.5 Finger positions of a gaita macho (from [1]).

Fig. 2.6 Approximation of the range of a gaita macho (from [1]).

The distance between the toneholes in a gaita hembra limits the player to be able to cover four toneholes at a time. Usually, the last tonehole (closest to the end) will be left open. In certain cases, the first tonehole, closest to the mouth, can be covered with a piece of wax, allowing the player to play with all the toneholes closed. In musical contexts, the gaita hembra is traditionally in charge of playing the melody, while the gaita macho

doubles or reinforces certain notes played by the hembra. Usually, the gaita macho is played keeping the tonehole closest to the mouthpiece closed all the time, using only positions 1 and 2.

2.2 Acoustics of Wind Instruments

Sound is produced in wind instruments by the oscillation of an enclosed volume of air. Oscillations are initiated —and sustained— by a player, who blows into the instrument in a particular way, depending on the instrument's particular mechanism [32]. In flutes and flute-like instruments, sound is produced by an air jet that flows across an opening at one end of the instrument. This section aims to review acoustic principles of wind instruments, focusing on flute-like instruments, such as the Colombian Gaita.

2.2.1 Sound Waves

Waves will propagate in any medium with mass and elasticity [31]. Gases such as air have no elastic resistance to shear, and acoustic waves that propagate in such media are primarily longitudinal—the displacement of the medium is parallel to the propagation of the wave [33].

Small sources will radiate sound in all directions in a nearly spherical way [31]. It is easier to start the study of these waves by looking at a small section of a wave at a large distance from the source, and treat it as a plane normal to the direction of propagation. For the purpose of this project, studying the propagation of waves in one dimension will suffice.

The one-dimensional wave equation referring to acoustic pressure p is defined as

$$\frac{\partial^2 p}{\partial t^2} = \frac{K}{\rho}\frac{\partial^2 p}{\partial x^2}, \tag{2.1}$$

where x is the spatial variable, t is the time variable, K is the bulk modulus and ρ is the density of air [31]. Similarly, the one-dimensional wave equation referring to acoustic displacement ξ is defined as

$$\frac{\partial^2 \xi}{\partial t^2} = \frac{K}{\rho}\frac{\partial^2 \xi}{\partial x^2}. \tag{2.2}$$

The relationship between speed of propagation c and the bulk modulus K can be expressed

as

$$c^2 = \frac{K}{\rho} = \frac{\lambda p_a}{\rho}, \tag{2.3}$$

where λ is the ratio of specific heats of air at a constant pressure and p_a is the atmospheric pressure. The wave equation relating pressure and position then becomes

$$\frac{\partial^2 p}{\partial t^2} = c^2 \frac{\partial^2 p}{\partial x^2}. \tag{2.4}$$

This substitution can also be applied to the wave equation for acoustic displacement ξ. Solutions to equation 2.1 describe the pressure evolution of one-dimensional plane waves propagating in air [7]. In the frequency domain, solutions to the one-dimensional wave equation moving in one direction have the form

$$p = \left[A e^{-j\omega \pm kx} \right], \tag{2.5}$$

where $k = \omega/c$ and A is the complex amplitude of the wave traveling in one direction. Writing the acoustic velocity $\partial \xi / \partial t$ as u, the pressure and velocity traveling wave components moving in the positive x direction are related by:

$$p^+ = \rho c u^+. \tag{2.6}$$

This relationship helps define the *wave impedance* or *specific impedance* in free space as

$$Z_c = \frac{p^+}{u^+} = \rho c. \tag{2.7}$$

2.2.2 Cylindrical Bores

Wind instruments make use of an air column whose natural frequencies must be properly aligned to set up regimes of oscillation in conjunction with the excitation mechanism. Different notes can be played on these instruments by changing the length of the resonant air column. This can be achieved by blowing into another pipe of different length, or by changing the effective length of the air column by placing a set of toneholes along the air column that can be opened and closed. Gaitas, as well as the Western family of woodwinds, fall into the second category. The lowest note of such instruments uses a regime

of oscillation based on the complete air column's vibrational mode acting in conjunction with higher modes. The higher notes of the low register are produced by opening holes one by one along the tube, beginning with the one farthest from the mouthpiece. This opening of the toneholes shortens the effective length of the air column, raising the frequency of the modes [10]. It is necessary that the ratio between the first mode and the subsequent normal modes of the instrument is independent of the length of the horn in order to maintain a similar *timbre* over the full range of the bore, and it also permits *overblowing*, the production of sounds based on higher order resonances [10].

Wave propagation as examined in section 2.2.1 refers to one-dimensional waves propagating in arbitrary contexts. This section explores wave propagation in cylindrical bores. The simplest system for study is an infinite cylindrical pipe with its axis parallel to the direction of propagation of a plane wave [31].

For the purposes of this thesis, it is not necessary to pursue an in-depth analysis of the three-dimensional wave equation. It will suffice to know that in a cylindrical tube, a mode will only propagate if the frequency exceeds a critical value or cutoff frequency. This cutoff frequency is 0 for the plane wave mode, so this mode will always propagate. The next mode of propagation has a cutoff frequency within the range of human hearing, but its excitation would require transverse circular motion, which will not be of significance in musical instruments. Therefore, wave motion in cylindrical tubes is primarily planar along the principal axis of the tube.

A pressure wave propagating along the primary axis of a cylindrical tube in the positive x direction has the form

$$p(x,t) = pe^{j(-kx+\omega t)}, \tag{2.8}$$

and the volume flow

$$U(x,t) = \frac{Sp}{\rho c} e^{j(-kx+\omega t)}, \tag{2.9}$$

where S is the cross sectional area of the tube. The characteristic, or wave impedance of the pipe can then be derived as

$$Z_c = \frac{p(x,t)}{U(x,t)} = \frac{\rho c}{S}. \tag{2.10}$$

This discussion so far has been restricted to infinite or semi-infinite cylindrical tubes.

For a finite cylindrical tube, waves will be partially reflected by a load impedance Z_L from the end, whether it is an open or closed pipe, defined as

$$\frac{p(L,t)}{U(L,t)} = Z_L. \tag{2.11}$$

For a pipe extending from $x = 0$ to $x = L$, terminated by the load impedance Z_L, the pressure in the pipe is a superposition of two waves, moving left and right with complex amplitudes A and B respectively [31].

The pressure wave *reflectance*, a frequency dependent reflection coefficient, is given by

$$\frac{B}{A} = e^{-2jkL}\left[\frac{Z_L - Z_c}{Z_L + Z_c}\right]. \tag{2.12}$$

If $Z_L = 0$ or $Z_L = \infty$, there will be no incidence of the pressure wave into the new medium, and the wave will be completely reflected, with a sign inversion in the first case. Conversely, if $Z_L = Z_c$, there will be no reflection.

The impedance at $x = 0$ or *input impedance* of the tube is given by

$$\begin{aligned} Z_{IN} &= \frac{p(0,t)}{U(0,t)} = Z_c\left[\frac{A+B}{A-B}\right] \\ &= Z_c\left[\frac{Z_L \cos(kL) + jZ_c \sin(kL)}{jZ_L \sin(kL) + Z_c \cos(kL)}\right]. \end{aligned} \tag{2.13}$$

The input impedance of an ideal open tube of finite length can be estimated using the low frequency approximation $Z_L = 0$, which reduces equation 2.13 to

$$Z_{IN} = jZ_c \tan(kL). \tag{2.14}$$

In an open-ended tube with the idealized condition that the input end $x = 0$ is also open, with $Z_{IN} = 0$, resonances are given by

$$f = \frac{nc}{2L}, \tag{2.15}$$

where n is an integer. The idealized open-open (open on both ends) pipe has a fundamental frequency with a wavelength of two times its length, and higher resonances at integer

multiples of the fundamental frequency [7]. The input impedance of an acoustic structure provides valuable information regarding its natural modes of vibration [7]. The instrument's transient response, tonal stability and dynamic range depend upon the extent to which the input impedance peaks are harmonically aligned [21].

2.2.3 Toneholes

Woodwind instruments use a series of toneholes along the acoustic tube of an instrument to change the effective length of the resonating air column, and therefore produce different pitches. Benade [10] defines a *tonehole lattice* (THL) as a potentially infinite sequence of toneholes. He points out that the acoustical behavior of a woodwind is very strongly influenced by the design of its system of toneholes. In his analysis, the toneholes are represented as T-sections, consisting of a piece of the main bore with radius a and length $2s$. Each T-section has at its center a side branch, a tonehole of radius b. The wall thickness is given by t. A pipe with this closed THL can be translated into a simpler shape, with the cross-sectional area enlarged by a factor E_c, , giving the effective cross sectional area to be

$$S_{E_c} = \pi a^2 \left[1 + \frac{1}{2} D^{(c)} \right],$$ (2.16)

for $D^{(c)} = \frac{1}{2}(b/a)^2(t/s) \ll 1$ and the length correction of a single T-section of the THL, given by [10]

$$E \approx 2s \left(\sqrt{1 + D^{(c)}} - 1 \right),$$ (2.17)

which can be added to the length correction of the other tonehole sections to find the length correction of the complete pipe. Open tonehole lattices also have an important role in the cutoff frequency, which is given by [7]

$$f_c = \frac{c}{2\pi s} \sqrt{\frac{D^{(o)}}{1 + \frac{2}{3}D^{(o)}}},$$ (2.18)

where $D^{(o)} = \frac{1}{2}(b/a)^2(s/t_e)$, and t_e is the effective length of the tonehole. Increasing the ratio of the tonehole and bore radii, (b/a), will raise the cutoff frequency of the open tonehole lattice.

A more detailed explanation of the characterization of toneholes in a cylindrical wood-

wind bore, as presented in [20] and refined in [21] is given in chapter 4.

2.2.4 Characterization of the response of air columns

The response of an air column can be characterized in both the frequency and the time domain. In the frequency domain, the input impedance $Z(f) = P(f)/U(f)$, is the complex ratio of pressure response, $P(f)$ to an input sinusoidal volume flow $U(f)$ into the entryway of the instrument. The minima of the input impedance in air-jet driven wind instruments occur at frequencies where sound production is favorable. Another frequency domain response is the reflection coefficient $R(f)$, defined as the complex ratio of the reflected pressure to an incident sinusoidal pressure into the air column [34]. The reflection coefficient describes how much of a wave is reflected back at an impedance discontinuity, such as a tonehole or the end of the instrument. In the time domain, air columns can be characterized by the impulse response $h(t)$. The impulse response is the pressure response at the entrance of the pipe to a unit volume flow impulse. The impulse response can be calculated indirectly as the inverse Fourier transform of the input impedance. After the initial impulse is sent, the input of the pipe is considered as a closed end. Another time domain characterization is the reflection function $r(t)$, defined as the reflected pressure response to a unit pressure impulse. After the initial impulse is sent into the entrance of the pipe, the input of the pipe is regarded as anechoic, so the impulse is not reflected back into the system. The reflection function decays much more rapidly than the impulse response. The reflection function can be calculated as the inverse Fourier transform of the reflection coefficient:

$$r(t) = FT^{-1}[R(f)]. \tag{2.19}$$

The impulse response is the time domain pressure response to the application of a volume velocity unit impulse at the input. The impulse response and the input impedance are time and frequency domain correlates:

$$Z(f) = FT[h(t)]. \tag{2.20}$$

The impedance and reflection coefficient of a system are related by the equation:

$$Z(f) = Z_c \frac{1 + R(f)}{1 - R(f)}. \tag{2.21}$$

2.2.5 The Air Jet Mechanism

This section offers a general description of the air jet mechanism in flue pipes. A more in-depth analysis of this mechanism would require an involved discussion of aeroacoustics and fluid dynamics, which is out of the scope of this work.

The excitation mechanism used by flutes, recorders and organ flue-pipes is controlled by a small jet of air that flows across —rather than directly into— an opening at one end of the instrument [10]. When the stream of air is directed across the opening at an adequate angle and pressure, an oscillatory flow of air will be set in motion, in and out of the instrument. Figure 2.7 illustrates this oscillatory flow of air into an organ flue pipe. The problem of the jet oscillation is quite complex and has been studied extensively theoretically and experimentally [32]. The excitation mechanisms of these types of instruments can have a fixed geometry (organ pipes, recorders) or a variable geometry (transverse flutes).

Three main elements need to be described for the modeling of the oscillation in flutes, the *jet receptivity*, the jet *instability* and the aeroacoustic sources. In a flute, the air jet is blown across an open end of the pipe. When acoustic oscillation occurs in the pipe, the jet instability synchronizes on the acoustic oscillation, resulting in a "forced" oscillation of the jet [3]. The hydrodynamic waves traveling on the jet have the same frequency as the acoustic oscillation. The jet oscillation grows as it is carried by the flow. Two characteristics of the jet motion are important for the oscillations of the instrument: the propagation velocity of the perturbation waves on the jet, and the amplification of the perturbation. These correspond to a characteristic growth factor of the instability waves along the jet [3], and they are both dependent on the frequency. At the labium (also known as upper lip in organ flue pipes, shown in Fig. 2.7), transverse perturbations of the jet are convected from the flue exit, and as a result, the jet oscillates from one side of the labium to the other. This induces a force on the labium, which is synchronized with the jet perturbation and the acoustic oscillation. The reacting force of the labium acts as an acoustic source that sustains the oscillation. The acoustic field in the pipe is responsible for the initial perturbation, which is convected and amplified due to the natural jet instability. The interaction of the perturbed jet with the labium is the aeroacoustic source that feeds
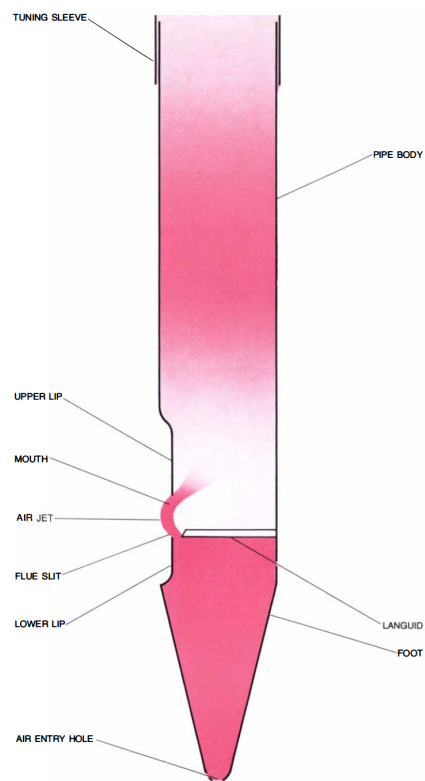
Fig. 2.7 Excitatory mechanism in a flue pipe [2].

energy into the pipe. As a response, the acoustic energy in the pipe is associated with the acoustic flow through the mouth, and results in the jet perturbation at the flue exit. The self-sustained oscillations in the instrument can be thought of as a feedback loop, as shown in Fig. 2.8.
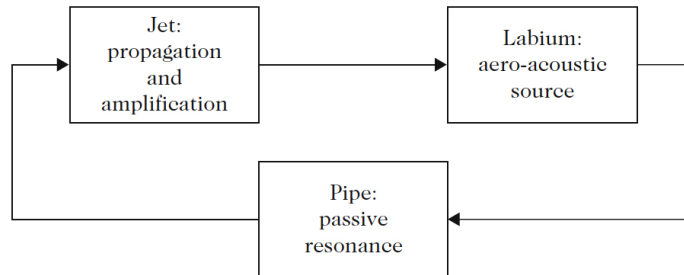
Fig. 2.8 Feedback loop describing self sustained oscillations in flutes [3].

In this loop, stationary oscillations can only take place when the total phase shift around the loop is a multiple of 2π. When blowing softly in a recorder, the time delay associated with the convection of the perturbations is about one half the period of oscillation. Therefore, the phase shift of the pipe response needs to be the complement of one period. By blowing harder, the jet velocity and the convection velocity increase. The phase shift due to the convection of perturbations on the jet decreases, so the oscillation frequency increases to match the phase condition. By blowing harder, the convection delay on the jet is eventually too small compared to the period of the resonance of the pipe, and the oscillation jumps to the next resonance [3], known as overblowing.

Chapter 3

Physical Modeling

Physical modeling synthesis looks to model and solve the physics of a system in order to synthesize its sound [35]. Unlike other synthesis methods, physical modeling can provide great expressive and parameter control, while being computationally efficient and requiring little memory. Physical modeling, however, requires a different model for each instrument or system being modeled. A musical oscillator is generally non-linear, but can be described in separate linear and non-linear mechanisms, as described by [4] and shown in Fig. 3.1. A non-linear element excites a linear, passive element. In the case of flue instruments, these mechanisms correspond to an air jet and an acoustic tube, respectively. The linear element, in turn, feeds back and influences the behaviour of the non-linear element.
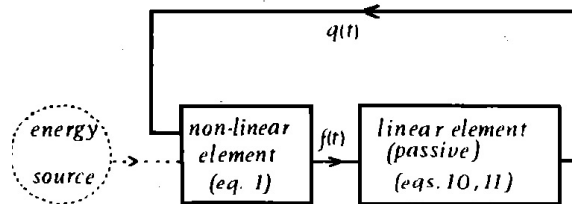
Fig. 3.1   Diagram of a fairly general musical oscillator (from[4]).

Physical models are usually one of two types: *lumped* or *distributed*. Lumped models consist of masses, springs and dampers (which can sometimes include non-linearities) and are usually used to simulate systems like the lips of a brass player or a piano hammer. Distributed models typically consist of transmission lines and distributed losses (which can

include non-linear components as well). A common, efficient technique to digitally model wave propagation in distributed systems is referred to as *digital waveguide modeling* [36], which makes use of digital delay lines and other digital filters to model wave propagation in strings, bores or acoustic spaces, among other systems. This chapter will focus on the latter, relying heavily on previous literature on digital waveguides, particularly in [6] and [7].

3.1 Physical Modeling using Digital Waveguides

Digital waveguides model the propagation and scattering of traveling waves in discrete-time accurately and efficiently. This section will review the fundamentals of this method with its applications to acoustic tubes.

3.1.1 Delay Lines

A digital delay line can be implemented by allocating a buffer of values in memory. It will introduce a delay of M samples between the input and its output, and will have the z-domain transfer function $H(z) = z^{-M}$. A diagram of an M-sample delay line is shown in Fig. 3.2. Integer-length delay lines can be trivially implemented, and non-integer delays can be implemented using interpolation techniques.

$$x[n] \longrightarrow \boxed{\qquad\qquad z^{-M} \qquad\qquad} \longrightarrow y[n]$$
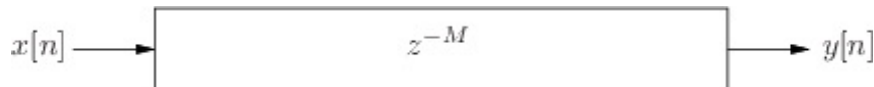
Fig. 3.2   An M-sample digital delay line (from [5]).

Interpolation algorithms must compute the output sample $y[n]$ which lies in between two samples at time M and $M + 1$ [37]. There exist several interpolation techniques for the implementation of fractional delay lines, including linear, spline, Lagrange and sinc interpolation. Two frequently used techniques for the implementation of delay-line interpolation are *linear interpolation* and *all-pass interpolation*. First-order linear interpolation is an efficient technique where the value at a fractional point between samples $y[n]$ and

$y[n-1]$ is given by:

$$
\begin{aligned}
y[n-\Delta] &= (1-\Delta) * y[n] + \Delta * y[n-1] \\
&= y[n] + \Delta(y[n-1] - y[n]).
\end{aligned}
\tag{3.1}
$$

The following is a block diagram for the implementation of first-order linear interpolation:
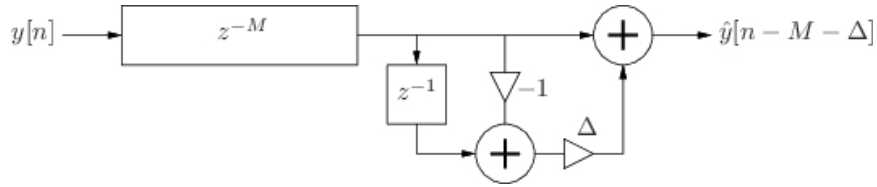
Fig. 3.3   Block diagram of first-order linear interpolation (from [5]).

First-order linear interpolation, also known as first-order Lagrange interpolation, becomes less accurate for high frequencies.

3.1.2 Modeling Wave Propagation Using Delay Lines

Delay lines can be used to simulate acoustic wave propagation. A simple delay line can be used to simulate any traveling wave that propagates in one direction with a fixed waveshape. The delay line length can be determined as $M = d/cT$, where $T = 1/f_s$ is the sampling period, c is the speed of sound and d is the distance of the listener from the source. If the wave attenuates at all frequencies by the same factor, the output of the delay can be scaled [6]. In general, these losses tend to be frequency dependent, and this damping can be commuted and implemented at discrete points in the system using a digital filter, as shown in Fig. 3.4.

Fig. 3.4   Simulation of a damped traveling wave, with losses commuted at the output (from [6]).

The air column of a cylindrical bore, such as a flute or a gaita, can be modeled using the one-dimensional wave equation (Eq. 2.1, as described in Section 2.2.1). This is usually

referred to as a *one-dimensional waveguide* [26]. A general solution to the wave equation is given by $y(x,t) = \left(A^{-jkx} + B^{jkx}\right)e^{j\omega t}$. Another solution to the wave equation in terms of traveling waves was presented by d'Alembert in 1747 as $y = y^+(ct - x) + y^-(ct + x)$ [5].

In the digital domain, it is necessary to sample the traveling wave amplitudes at intervals of T seconds. The spatial sampling interval corresponds to the distance traveled by sound in one temporal sampling interval. Each component of the traveling wave moves left or right one spatial sample for each time sample [7]. By substituting sampled variables for continuous variables

$$
\begin{aligned}
x &\longrightarrow x_m = mX \\
t &\longrightarrow t_n = nT_s,
\end{aligned}
\tag{3.2}
$$

the traveling wave solution then becomes

$$
\begin{aligned}
y(x_n, x_m) &= y^+(t_n - x_m/c) + y^-(t_n + x_m/c) \\
&= y(nT_s - mX/c) + y^-(nT_s + mX/c) \\
&= y^+[(n - m)T_s] + y^-[(n + m)T_s].
\end{aligned}
\tag{3.3}
$$

A further simplification results in

$$
y(t_n, x_m) = y^+(n - m) + y^-(n + m),
\tag{3.4}
$$

an expression for physical displacement at time n and location m, as the sum of two traveling wave components. This is a most basic waveguide, defined by [6] as a bidirectional delay line at some wave impedance.

3.1.3 Digital Waveguides

Each delay line will contain a sampled traveling wave, moving left or right. From the previous equation, the term $y^+(n - m)$ can be thought of as the output of an M-sample delay line with input $y^+(n)$, while the term $y^-(n + m)$ can be thought of as the input of an M-sample delay line with output $y^-(n)$ [26]. The right and left-going components of the traveling wave must be then summed to produced the physical output $y(t_n, x_m)$. In this way, a bidirectional delay line, or digital waveguide, can model any one-dimensional linear acoustic system, such as a string or a bore. This basic waveguide structure is shown in Fig.

3.5.
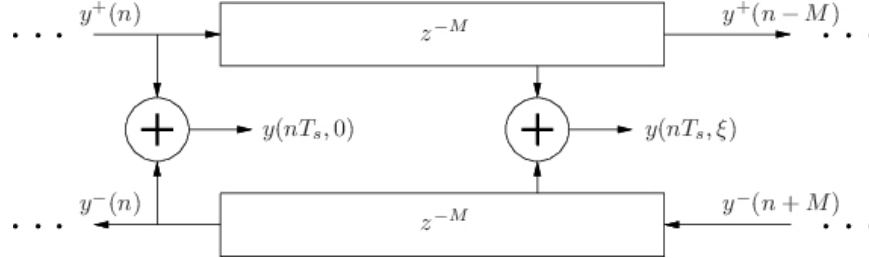
Fig. 3.5 Diagram of a digital waveguide (from [5]).

3.2 Modeling of Wind Instruments

Traditionally, acoustic tubes were characterized in the frequency domain. Good shapes for bores and toneholes have been rationalized by considering the relationships between the normal mode frequencies that are favorable for periodic oscillations. A characterization in the time domain, however, proves advantageous in terms of computational expense. Research on the non-linear excitation mechanisms of wind instruments has also advanced the development of time-domain models [3, 18].

The time-domain response of an acoustic tube can be represented in terms of its *reflection function*, $r(t)$ or its *impulse response*, $h(t)$. The impulse response is the pressure response at the bore entrance after a unit volume velocity impulse is introduced at the entrance, with the boundary at the entrance subsequently assumed to be rigid (or closed). The reflection function is the pressure response at the entrance of the tube after a unit pressure impulse is sent out, with no reflections at the entry point.

3.2.1 Modeling of Cylindrical Bores

The two commonly used waveguide variables for acoustic tube simulation are pressure and volume velocity, analogous to force and transverse velocity in strings.

The Ohm's law relations for acoustic tube variables are given by:

$$p^+(n) = Z_c u^+(n) \tag{3.5}$$

$$p^-(n) = -Z_c u^-(n), \tag{3.6}$$

where p^+ and p^- are the right- and left-going pressure components, respectively, u^+ and u^- are the right- and left-going volume velocity components, respectively, and Z_c is the acoustic wave impedance, given by:

$$Z_c = \frac{\rho c}{A}. \tag{3.7}$$

Here, ρ is the density of air, c is the speed of sound in air and A is the cross sectional area of the acoustic tube.

Using the one-dimensional equation for plane waves (Eq. 2.1) and the discrete-time solution (Eq. 3.4) we can represent the lossless wave propagation along the central axis of a cylindrical tube using the digital waveguide structure shown in Fig. 3.5.

The reflectance, observed from the entrance of the cylindrical tube of length L is given by:

$$\mathcal{R}(\Omega) = e^{-2jkL} \left[\frac{Z_L(\Omega) - Z_c}{Z_L(\Omega) + Z_c} \right], \tag{3.8}$$

where Z_c is the real characteristic wave impedance of the pipe, and $Z_L(\Omega)$ is the load impedance at $x = L$. For $Z_L = 0$, corresponding to zero pressure at $x = L$, $\mathcal{R}(\Omega) = -e^{-2jkL}$. The continuous-time reflection function is found as the inverse Fourier transform of $\mathcal{R}(\Omega)$, when viscothermal losses are ignored [7]. Figure 3.6 shows the implementation of this digital waveguide structure with an arbitrary load impedance.
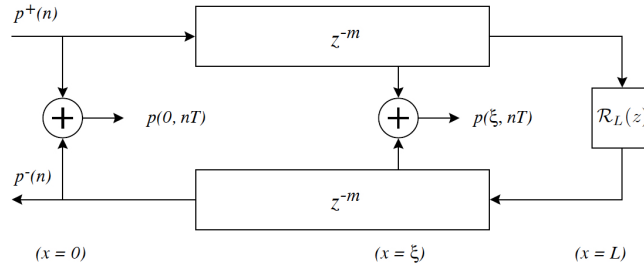
Fig. 3.6 Digital waveguide implementation of plane wave propagation in a cylindrical tube (from [7]).

This waveguide structure can be simplified by limiting the observation point to the entry of the bore. In this way, we can use one single delay line and the digital filter used to represent the reflectance can be pushed through the lower delay line by linearity and time-invariance [7], as shown in Fig. 3.7.
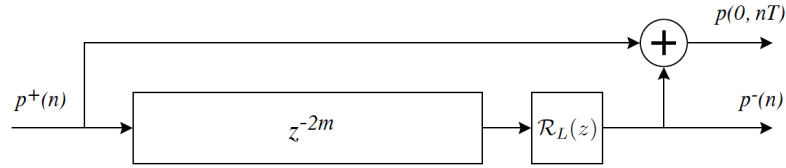
Fig. 3.7 Digital waveguide of an ideal cylindrical tube using a single delay line (from [7]).

The waveguide input impedance can be found by calculating the impulse response of the system, and transforming it to the frequency domain using the Discrete Fourier Transform (DFT), using the structure shown in Fig. 3.8.
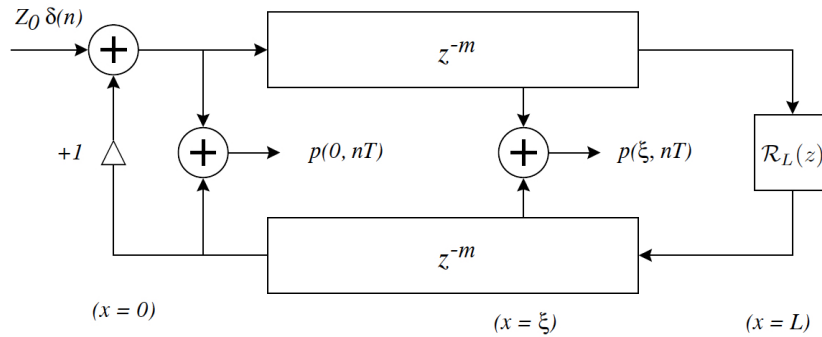
Fig. 3.8 Digital waveguide model of a closed-open cylindrical bore (from [7]).

Figure 3.9 shows the input impedance and impulse response of a digital waveguide model of a cylindrical bore of length 84.79cm and radius 6.6mm, implemented using a single non-interpolating delay line, and an approximation of the reflectance using a second order IIR filter based on the results from Levine & Schwinger unflanged cylindrical bore reflectance [38], designed using *openpipe.m* from [7].

3.2.2 Modeling of Toneholes

Various models have been proposed to characterize toneholes in the time and frequency domains. We make use of the approach presented in [7, 8], which is summarized in the following paragraphs. Keefe [21] describes a model for a tonehole unit where acoustic variables are related by a transmission matrix of series and shunt impedance parameters.
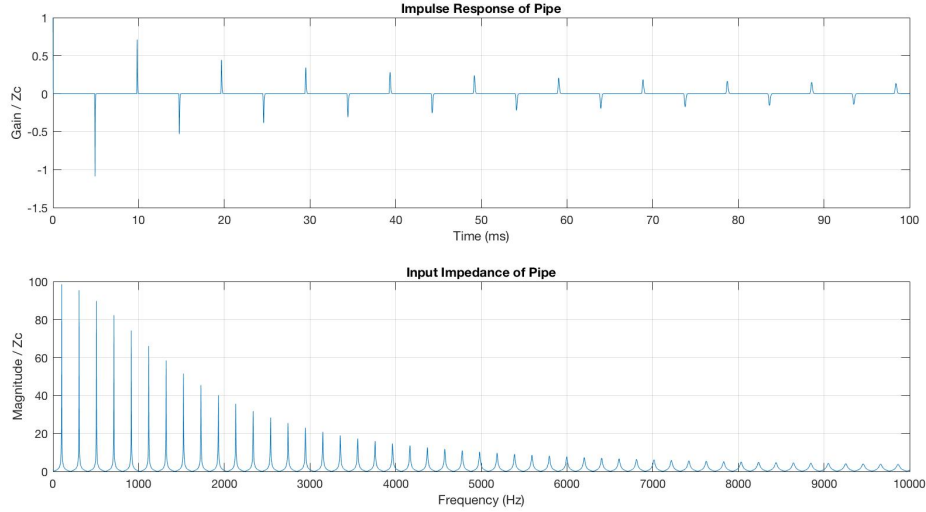
Fig. 3.9 Impulse response (top) and input impedance (bottom) of a digital waveguide model of a cylindrical bore of radius 6.6mm and length 84.79cm. End reflection filter approximated using *openpipe.m* from [7].

Keefe's original derivation was based on a symmetric T-section. The shunt impedance Z_s results from an analysis of a pressure anti-node at the junction, where pressure is symmetric and equal across the junction. The series impedance terms result from an analysis of a pressure node at the tonehole junction, where volume flow is symmetric and equal across the junction. The resulting transmission matrix is:

$$\begin{bmatrix} P_1 \\ U_1 \end{bmatrix} = \begin{bmatrix} 1 & Z_a/2 \\ 0 & 1 \end{bmatrix} \begin{bmatrix} 1 & 0 \\ Z_s^{-1} & 1 \end{bmatrix} \begin{bmatrix} 1 & Z_a/2 \\ 0 & 1 \end{bmatrix} \begin{bmatrix} P_2 \\ U_2 \end{bmatrix} \tag{3.9}$$

$$= \begin{bmatrix} 1 + \frac{Z_a}{2Z_s} & Z_a(1 + \frac{Z_a}{4Z_s}) \\ Z_s^{-1} & 1 + \frac{Z_a}{2Z_s} \end{bmatrix} \begin{bmatrix} P_2 \\ U_2 \end{bmatrix}.$$

This equation can be reduced based on the approximation that $|Z_a/Z_s| \ll 1$, resulting in the basic tonehole unit cell given by Keefe for transfer-matrix function calculations [21]:

$$\begin{bmatrix} P_1 \\ U_1 \end{bmatrix} = \begin{bmatrix} 1 & Z_a \\ Z_s^{-1} & 1 \end{bmatrix} \begin{bmatrix} P_2 \\ U_2 \end{bmatrix}. \tag{3.10}$$

In order to render these relationships in the digital waveguide domain, it is necessary to transform the plane-wave transmission matrix coordinates of pressure and volume velocity to waveguide coordinates [7]:

$$\begin{bmatrix} P_1 \\ U_1 \end{bmatrix} = \begin{bmatrix} P_1^+ + P_1^- \\ Z_c^{-1}(P_1^+ - P_1^1) \end{bmatrix},$$

(3.11)

where Z_c is the characteristic impedance of the bore, equal at both sides of the tonehole. This relates waveguide pressure variables as follows:

$$\begin{bmatrix} P_1^- \\ P_2^+ \end{bmatrix} = \begin{bmatrix} \mathcal{R}^- & \mathcal{T}^- \\ \mathcal{T}^+ & \mathcal{R}^+ \end{bmatrix} \begin{bmatrix} P_1^+ \\ P_2^- \end{bmatrix}.$$

(3.12)

The structure shown in Fig. 3.10 shows the resulting continuous-time reflectance and transmittance terms, which must be converted into appropriate discrete time representations. A sequence of toneholes is then represented as shown in Fig. 3.11.
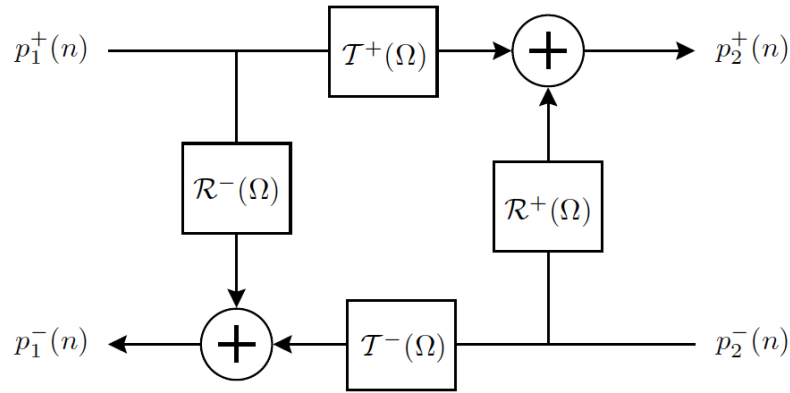
Fig. 3.10 Digital waveguide tonehole two port scattering junction (from [7]).

A two-port tonehole scattering junction has the disadvantage of having only an open or closed characterization of the tonehole, which cannot be efficiently unified in a single tonehole model.

A tonehole can also be modeled using a three-port scattering junction. Välimaki [27] proposed a three-port tonehole model in which a side branch is connected to a uniform cylindrical bore. Scavone [8] describes a three-port scattering junction characterization of a tonehole, in which the fixed portions of the tonehole are separated from the variable

Fig. 3.11 Digital waveguide implementation of series of two-port toneholes (from [8]).

components. This method models the shunt impedance term of the Keefe tonehole characterization. The characterization of the open/closed tonehole end can be efficiently modeled by a simple inertance model. The impedance of the open end is given by:

$$Z_e^{(o)}(s) = \frac{\rho t}{S_e} s, \tag{3.13}$$

where S_e is the cross-sectional area of the end hole, t is the effective length of the opening, and s is the Laplace transform variable. The open-end reflectance is:

$$\mathcal{R}_e^{(o)} = \frac{P_e^-(s)}{P_e^+(s)} = \frac{Z_e^{(o)}(s) - Z_{cb}}{Z_e^{(o)}(s) + Z_{cb}} = \frac{ts - c}{ts + c}, \tag{3.14}$$

where Z_{cb} is the characteristic impedance of the tonehole branch. An appropriate discrete-time filter implementation can be obtained using the bilinear transform mapping from the s-plane to the z-plane, resulting in:

$$\mathcal{R}_e^{(o)}(z) = \frac{a - z^{-1}}{1 - az^{-1}}, \tag{3.15}$$

where

$$a = \frac{t\alpha - c}{t\alpha + c}, \tag{3.16}$$

and α is the bilinear transform constant which controls frequency warping [8]. A low-frequency discrete-time fit is achieved for $\alpha = 2f_s$ [7]. The discrete-time reflectance is a

first order allpass filter. The closing of the tonehole can be simulated by taking the hole radius smoothly to zero, in which case the allpass coefficient will be set to a value nearly equal to one, which corresponds to the pressure reflection at a rigid termination. Figure 3.12 shows a diagram of the implementation of the three-port scattering junction.
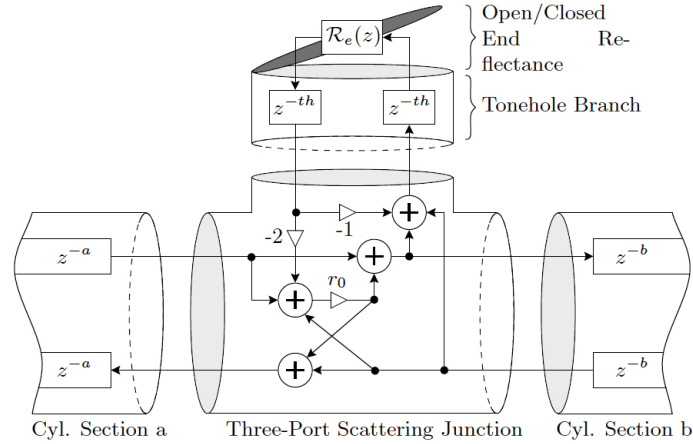
Fig. 3.12   Digital waveguide implementation of a three-port tonehole scattering junction (from [8]).

The scattering coefficient is defined as:

$$r_0 = \frac{-Z_c}{Z_c + 2Z_{cth}}. \tag{3.17}$$

In this way, a series of toneholes can be implemented by using appropriately sized delay lines on the sides of the scattering junctions. This part of the model covers the linear passive element shown in Fig. 3.1.

3.2.3 Modeling of Air Jets

Modeling the non-linear excitation mechanism of flue instruments is a non-trivial task. The underlying physics of the volume flow are complex in nature, and an exact simulation of the fluid dynamic phenomena requires a large amount of computing power, not suitable for real-time synthesis [12].

The non-linear element shown in Fig. 3.1 was described in [4] as:

$$f(t) = F(q\{t - \tau\}), \tag{3.18}$$

where the term τ implies a time delay in the volume flow displacement, since the air has to travel a small distance before it hits the labium of the instrument. The interaction of the air jet with the tube can be described in terms of a non-linear function called a sigmoid function. One such function of volume displacement, as shown in Fig. 3.13, is of the form:

$$F(q) = h + k \tanh(lq), \tag{3.19}$$

where k is a gain term and h is an offset from the center of the labium. Here, a value of 0 for h will produce weak even harmonics, as the air would blow into the labium exactly in the middle, and changing this parameter can introduce more even harmonics.
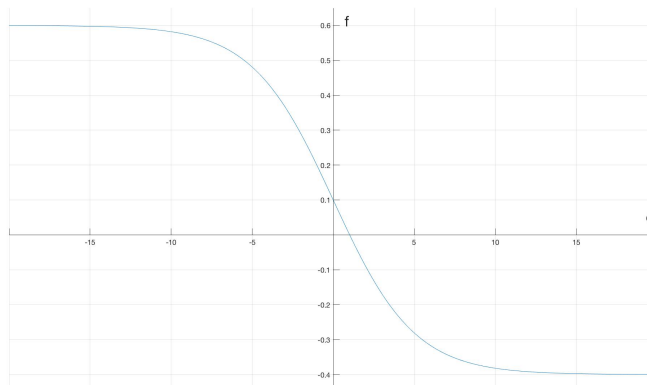
Fig. 3.13   Non-linear characteristic for a an air jet, as described in [4].

For the simulation of pressure, as opposed to volume flow, a sigmoid function of the form

$$p^+ = x^3 - x, \tag{3.20}$$

as shown in Fig. 3.14, has been used in [28] and [9].

Figure 3.15 illustrates the air jet excitation mechanism in a flute. In this diagram, t_s denotes the width of the air jet, and d_s the physical distance the air must travel before reaching the labium of the instrument. A delay line is used to represent this distance in the models discussed so far. The length of this delay line, which is placed before the sigmoid function, is not derived physically, as the speed of the disturbance of the jet is slower than the speed of the jet itself. As mentioned in Chapter 2, certain relations between the transit
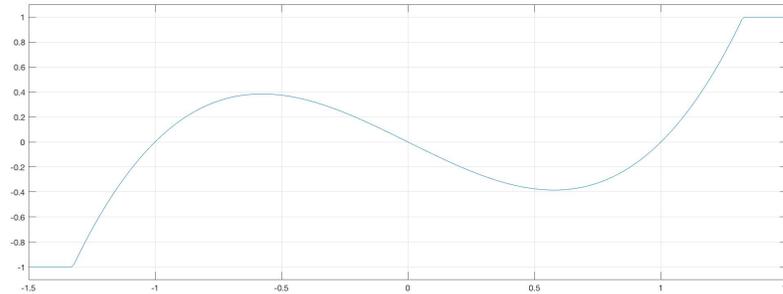
Fig. 3.14   Non-linear characteristic for a an air jet, as implemented in [9].

time and the period of oscillation of higher partials of the tone allow these partials to enter actively into the regime of oscillation [10]. Depending on the particular geometry of the instrument, the player might have more than one way of modifying the transit time, such as a shorter or longer distance d_s or a larger or smaller flow velocity and thickness/width of the air stream. In a digital waveguide model, however, we do not have control over these physical phenomena. In order to simulate the change of transit time or flow velocity, we can modulate the length of the delay line representing the jet, which will excite different modes in the model.
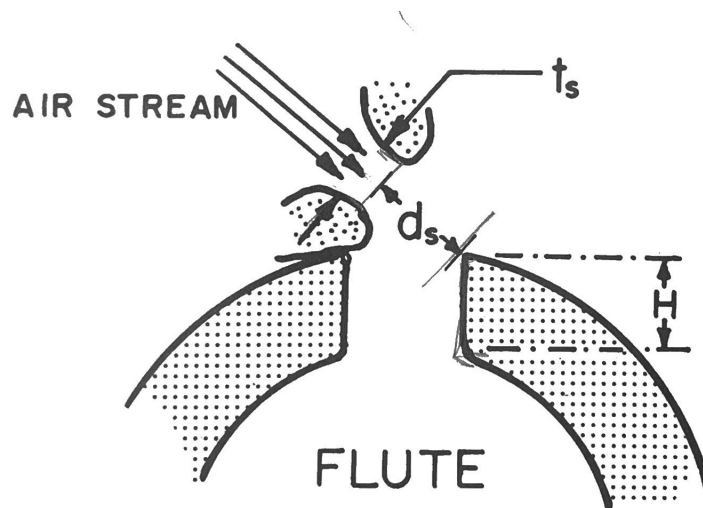
Fig. 3.15   Air jet excitation mechanism in a flute (from [10]).

Figure 3.16 shows the diagram of the implementation of the flute included in the STK

[11] distribution. In this model, the fundamental frequency is set by changing the length of the delay line representing the acoustic tube.
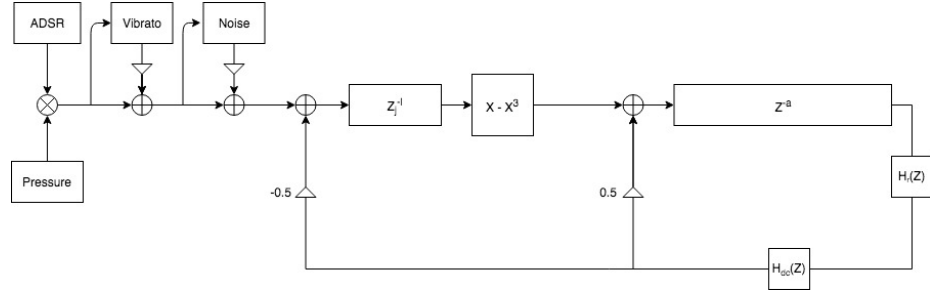
Fig. 3.16 Digital waveguide implementation of a flute, included in the STK [11].

Verge et. al [12] proposed another real-time simulation model for recorder-like instruments that takes into account the effects on sound production by the instrument of the jet oscillations, vortex shedding at the edge of the instrument and turbulence at the mouth. In this model, the tube is represented by a large tube of cross section $S_p = H^2$ and length $L_p + \delta_p$, where L_p is the length of the pipe and δ_p is the end correction associated with the open pipe termination. The mouth of the instrument is represented by a smaller tube of cross section $S_m = WH$ where W is the distance between the flue exit and the labium. The complicated two-dimensional geometry of the mouth of the instrument can then be represented by an equivalent pipe segment of length δ_m. The one-dimensional reduction is shown in 3.17.

The model is driven by a pressure signal p_f representing the pressure in the foot of the organ pipe or the mouth of the musician. The model uses the Bernoulli equation to relate the pressure drop across the flue canal $p_f - p_m$ with the resulting jet velocity U_j:

$$\rho_0 l_c \frac{dU_j}{dt} + \frac{1}{2}\rho_0 U_j^2 = p_f - p_m, \tag{3.21}$$

where ρ is the air density, l_c is the length of the flue canal and t is time. The jet oscillation of the model uses a modification of the semi-empirical formula by Fletcher and Thwaites for laminar jets:

$$\eta(W, \omega) = \frac{1}{i\omega}\left(\frac{2}{\pi}\frac{Q_p}{S_m}\frac{0.38Q_1'}{S_m}\right) \times \left[1 - \cosh\left(\mu W\right)\exp\left(\frac{-i\omega W}{u}\right)\right]. \tag{3.22}$$
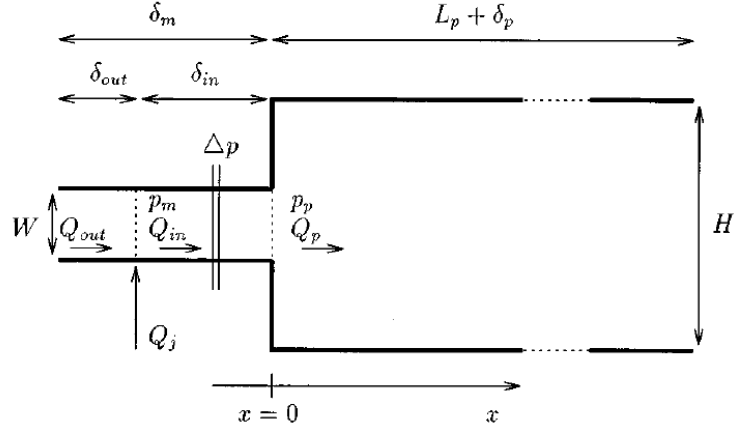
Fig. 3.17 One-dimensional reduction used to simulate recorder-like instruments in [12].

Here, W is the distance between the flue exit and the edge of the labium, $\mu(St)$ is an amplification coefficient, $u(St)$ is the speed of the hydrodynamic perturbation on the jet, and St the Strouhal number. Q_1' is defined as:

$$Q_1' = Q_1 - \frac{1}{2}bHU_0. \tag{3.23}$$

The full model proposed by Verge et al. [12] can be described with the following equation:

$$p_o = \frac{r^2 S_p}{4c_0^2 S_m}\frac{\partial(p_o - p_i)}{\partial t^2} - \frac{\rho_0 r_m^2}{4c_0 S_m}\frac{d^2 Q_j}{dt^2} - \frac{\delta m S_p}{c_0 S_m}\frac{\partial(p_o - p_i)}{\partial t} + \frac{\rho \delta_{out}}{S_m}\frac{dQ_j}{dt} + \Delta p - p_i. \tag{3.24}$$

The pressure jump term Δp in the equation includes the different sound-producing mechanisms at the edge of the labium:

$$\Delta p = \Delta p_{jd} + \Delta p_a + \Delta p_{tr} + \Delta p_t, \tag{3.25}$$

where Δp_{jd} corresponds to the jet-drive mechanism, Δp_a and $\Delta p_t r$ to vortex shedding at the edge of the labium and Δp_t to turbulence. An implementation of this recorder model, shown in Fig. 3.18, developed by Mathias Bredholt at McGill University is available in the latest update of the STK [11].
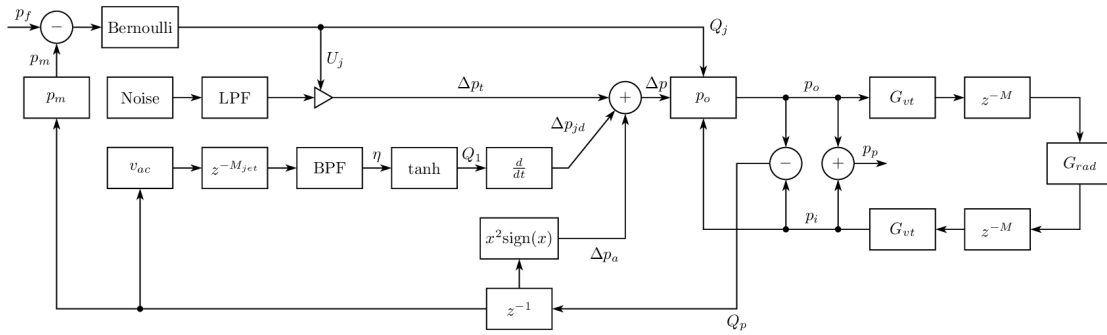
Fig. 3.18   STK implementation of the model developed by Verge et al. in [12].

3.3 Conclusion

Recalling the general definition of a musical oscillator presented in [4] and shown in Fig. 3.1, we can describe and model the gaita in terms of a linear element, the acoustic tube, and a non-linear element, the air jet excitation mechanism. In this chapter, some physical modeling techniques to model these elements have been reviewed. In addition, a technique for modeling the toneholes of an acoustic tube has also been described. The model developed and implemented in this thesis, and detailed in Chapter 5, will make use of the techniques presented in this chapter.

Chapter 4

Physical Measurements of a Gaita

4.1 Dimensions
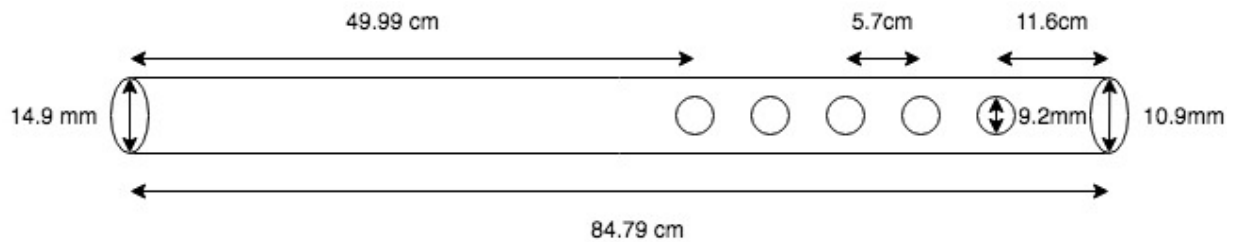
Fig. 4.1   Physical measurements of the bore of a gaita hembra.

Figure 4.1 illustrates the dimensions of the instruments used in this project. As mentioned in Chapter 2, gaitas are traditional instruments built in an artisanal way. Because of this, the physical dimensions will vary between instruments. Depending on the natural shape of the cardón used, the radius of the instrument will vary as well. Cardón is usually slightly conical, therefore the impedance measurement and comparison with theoretical models serve to assess if the behavior of the instrument could be approximated using a cylindrical bore model.

The distance between toneholes has variations in the order of 2 mm. The diameter of the toneholes also have variations in the order of 0.13 mm. The input end of the instrument has a diameter of 14.9 mm, while the opposite end of the instrument is smaller, with a diameter of 10.9mm.

4.2 Impedance Measurements

The input impedances of a pair of gaitas with different fingering positions was measured in order to visualize their response and compare it to the response of the theoretical model. The head of the instruments was removed using a heat gun to soften the wax. A first set of measurements was taken at the Computational Acoustic Modeling Laboratory (CAML) at McGill University, using a Capteur d'impédance system [39], developed at the Centre de Transfert de Technologie du Mans and the Laboratoire d'Acoustique de l'Université du Mans, and a second set of measurements were taken using the zProbe system at CAML [40].

The zProbe system consists of an impedance head with 6 PCB 377B10 condenser microphones and 426B03 preamplifiers, a JBL 2426H compression driver, a calibration pipe and a rack containing an RME Fireface 800 audio interface and a PCB 483C15 signal conditioner. An adaptor for the gaitas was 3-D printed with the help of Song Wang at CAML. The zProbe is used with a MATLAB program available at CAML. Figure 4.2 shows the impedance measurement of a gaita hembra with all of the holes closed, from the first set of measurements.
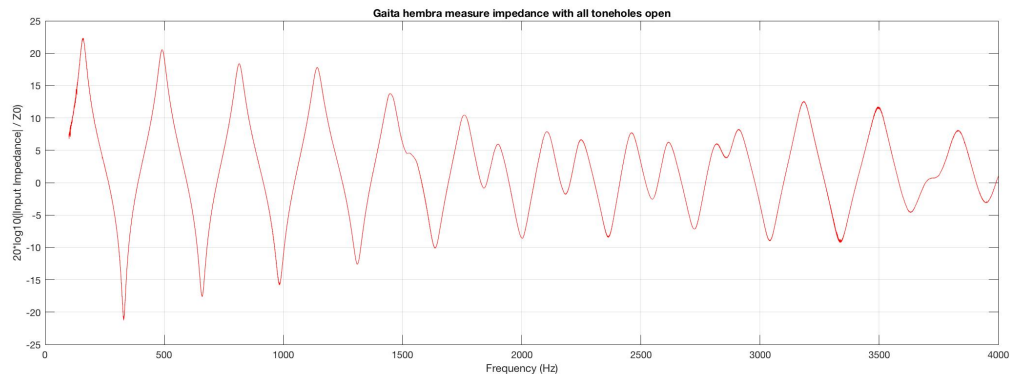
Fig. 4.2   Measured input impedance of a gaita hembra, all toneholes open.

For more information about the Capteur d'impédance and zProbe systems the reader can refer to [39], [41], [42], and [43].

4.3 The Transfer Matrix Model

Chapter 3 introduced the description of a tonehole unit by Keefe in [21]. In this model, acoustic variables are related by a transmission matrix of series and shunt impedances. This woodwind air column model can be used to analyze the properties of existing instruments and to construct time-domain simulations of woodwinds [21]. Using this model and the physical dimensions of the gaitas, the theoretical impedance and impulse response of the instruments can be calculated. By comparing the theoretical response of the instrument and the actual measurements, we can determine if a cylindrical model is a suitable representation for the instrument.

For an arbitrary two port acoustical system, the transfer matrix for wave propagation that maps the input volume flow u_1 and pressure p_1 to the output volume flow u_0 and pressure p_0 is defined as:

$$\begin{bmatrix} p_0 \\ u_0 \end{bmatrix} = \begin{bmatrix} a & b \\ c & d \end{bmatrix} \begin{bmatrix} p_1 \\ u_1 \end{bmatrix}, \tag{4.1}$$

where the matrix composed of A, B, C and D results from the cascading of the transfer matrices for the elements of the system, in this particular case, the acoustic tube sections and the toneholes [21].

The transfer matrix for a cylindrical tube, taking into account visco thermal losses factor is given by [21]:

$$T_b(x, a) = \begin{bmatrix} \cosh \Gamma x & Z_c \sinh \Gamma x \\ Z_c^{-1} \sinh \Gamma x & \cosh \Gamma x \end{bmatrix}, \tag{4.2}$$

where x is the length of the acoustic tube of radius a and Γ is the complex propagation constant.

The transfer matrices for open and closed toneholes, as already discussed in Chapter 3, given $|Z_a/Z_s| \ll 1$, are given by equations 4.3 and 4.4 respectively.

$$T_h^{(o)} = \begin{bmatrix} 1 & Z_a^{(o)} \\ 1/Z_s^{(o)} & 1 \end{bmatrix} \tag{4.3}$$

$$T_h^{(c)} = \begin{bmatrix} 1 & Z_a^{(c)} \\ 1/Z_s^{(c)} & 1 \end{bmatrix}. \tag{4.4}$$

In order to calculate the theoretical response for a given geometry, the model takes into account several physical parameters. In terms of the bore, these parameters are the radius of the bore at both ends and total length. In terms of each tonehole, the parameters are distance from the input end, radius, tonehole height, protrusion from the bore, and, if padding exists, its radius and height. For the gaitas, the padding parameters can be left out. As the toneholes in gaitas are drilled into the instrument, the protrusion parameter is set to 0, and the tonehole height parameter is set equal to the thickness of the wall of the instrument. Three matrices are used in the *MATLAB* script: the first for the bore data, the second for the tonehole data and the third for the tonehole states. From these matrices we can calculate the characteristic impedance of each tonehole and each bore section, given by equation 3.7. Having the previous data, we can calculate the input impedance of the system by working our way back from load impedance at the end of the instrument.

For the open end, we calculate the radiation impedance. The radiation impedance is related to the reflection coefficient by

$$Z_r = Z_c \frac{1 + R}{1 - R}. \tag{4.5}$$

In an unflanged pipe, the modulus of the reflection coefficient $|R_0|$ can be approximated as

$$|R_0| = \frac{1 + \alpha ka + \beta(ka)^2}{1 + \alpha ka + (\frac{1}{2} + \beta(ka)^2)}, \tag{4.6}$$

with $\alpha = 0.2$ and $\beta = -0.084$ for $ka < 3.5$ [44]. The reflection coefficient is then given by

$$R = -|R_0|e^{-2jk\tilde{\delta}}, \tag{4.7}$$

where $\tilde{\delta}$ is the frequency dependent length correction of the pipe. [45] propose the following equation for the length correction $\tilde{\delta}_0$

$$\tilde{\delta}_0 = \delta_0 \left[\frac{1 + 0.044(ka)^2}{1 + 0.19(ka)^2} - 0.02 \sin^2 (2ka) \right], \tag{4.8}$$

with $\delta_0 = 0.6133a$ for $ka < 1.5$ [45]. Having calculated the radiation impedance, we can

calculate the load impedance Z_L at the end of the tube, and move back to calculate the transmission matrices of the toneholes and tube sections, given by Eqs. 4.2, 4.3 and 4.4. The complex propagation constant in Eq. 4.2 is given by [46]:

$$\Gamma = \frac{\omega}{c} + (1+j)\alpha, \tag{4.9}$$

where

$$\alpha = 2.96 \times 10^{-5} \sqrt{f}/a. \tag{4.10}$$

[45]

Next, we can calculate the impedance of the last tonehole, using Eq. 4.3 or 4.4 depending on the state of the hole. The series and shunt impedances for open and closed states are given by [23]

$$Z_s^{(o)} = Z_c \delta^2 (jkt_s^{(o)} + \xi)$$

$$Z_s^{(c)} = -jZ_c \delta^2 \cot kt_s^{(c)}$$

$$Z_a^{(o)} = -jZ_c \delta^2 kt_a^{(o)}$$

$$Z_a^{(c)} = -jZ_c \delta^2 kt_a^{(c)}, \tag{4.11}$$

where Z_c is the characteristic impedance of the tonehole, δ is the ratio of the radius of the tonehole (b) to the radius of the main bore (a). t_s and t_a are equivalent lengths, m and ξ is the specific resistance, characterizing radiaton losses when the tonehole is open [23]. A low frequency approximation for ξ is given in [47] as $\xi = (kb)^2/4$. To evaluate $Z_s^{(o)}$, [47] propose:

$$Z_s^{(o)} = jZ_c\{kt_i + \tan[k(t + t_m + t_r)]\}, \tag{4.12}$$

where t is the physical height of the tonehole, t_i is the inner length correction, t_m is the matching volume length correction, and t_r is the radiation length correction. The inner length correction and matching volume length corrections are given by [24] as

$$t_i = (0.84 - 1.4\delta^2 + 0.75\delta^{2.7})b \tag{4.13}$$

$$t_m = \frac{b\delta}{8}\left(1 + 0.207\delta^3\right). \tag{4.14}$$

The radiation length correction t_r is obtained from the radiation impedance of the hole [23]

$$t_r = \arctan\left[Z_r/(jZ_c)\right]/k, \tag{4.15}$$

a model of an unflanged pipe in the low frequency approximation is adequate [23]

$$Z_r = Z_c\left[0.25(kb)^2 + jk0.61b\right]. \tag{4.16}$$

Fit formulas for the series length correction were proposed by [23] as

$$t_a^{(o)} = b\delta^2(-0.35 + 0.06\tanh\{2.7t/b\}) \tag{4.17}$$

$$t_a^{(c)} = b\delta^2(-0.12 - 0.17\tanh\{2.4t/b\}). \tag{4.18}$$

After calculating the coefficients for the tonehole transfer matrix, we work our way back to calculate the previous tonehole and bore section coefficients. The transfer matrices can be then cascaded as

$$\begin{bmatrix} P_0 \\ U_0 \end{bmatrix} = \begin{bmatrix} A & B \\ C & D \end{bmatrix}\begin{bmatrix} P_L \\ U_L \end{bmatrix}, \tag{4.19}$$

where

$$\begin{bmatrix} A & B \\ C & D \end{bmatrix} = \prod_{i=1}^{n}\begin{bmatrix} a_i & b_i \\ c_i & d_i \end{bmatrix}. \tag{4.20}$$

The input impedance of the acoustic system can be calculated as follows:

$$Z_{in} = \frac{B + AZ_L}{D + CZ_L}. \tag{4.21}$$

These calculations were made using MATLAB scripts by Gary Scavone available at the Computational Acoustic Modeling Laboratory.

4.4 Comparison of measurements

4.4.1 Gaita Hembra

The measurements were made on six different tonehole state configurations, which correspond to the fingerings used on the instrument, starting from having all toneholes closed, and opening one hole on every subsequent measurement starting from the farthest from

the input end. The second set of measurements, using the zProbe system were used in this section.

For a gaita hembra with all toneholes closed, the impedance response is closely related to the theoretical model. The peaks of the impedance response are quite close in frequency. Most peaks are aligned in the range +-4 Hz, with some differences in amplitude. The difference in amplitude is more significant in the fundamental, with a difference of 4 dB. Other peaks show a difference of +-1 dB. The reflection from the end of the bore differs by .05 ms.
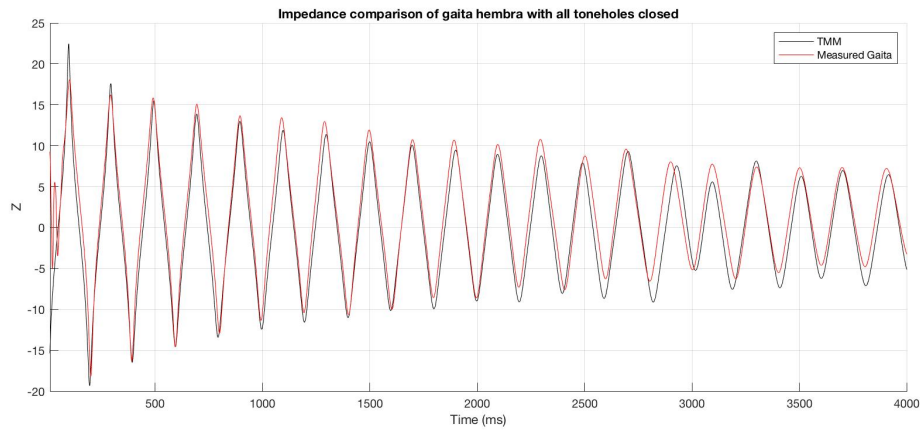
Fig. 4.3   Comparison between the theoretical input impedance of the Transfer Matrix Model and the measurements of a gaita hembra with all toneholes closed.
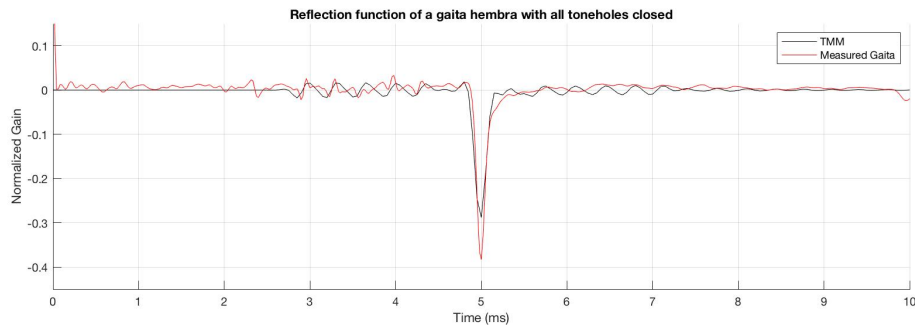
Fig. 4.4   Comparison between the theoretical reflection function of the Transfer Matrix Model and the measurements of a gaita hembra with all toneholes closed.

For the gaita hembra with four toneholes closed we also observe a close correspondence between the impedance of the theoretical model and the measurements. The first resonance

is 4dB higher in the theoretical model and decays slightly faster than the measurements. The frequencies of the modes of the theoretical model are shifted a few Hz compared with the measurements, though this is likely due to differences in the measured and modeled temperatures.
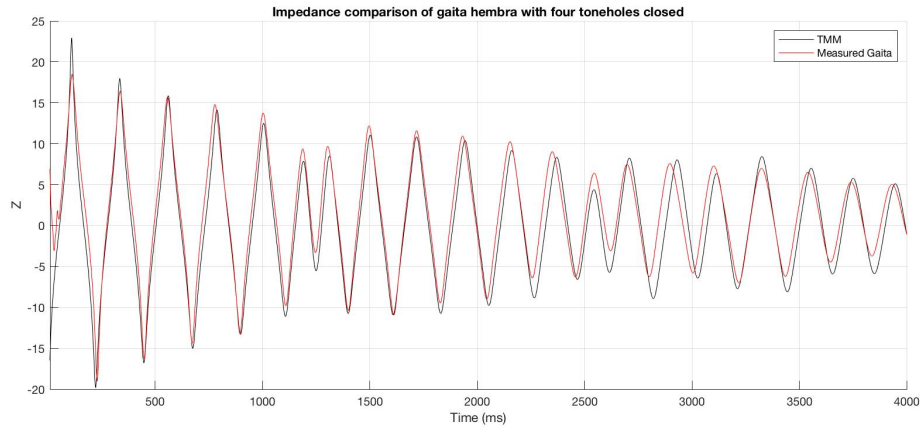
Fig. 4.5   Comparison between the theoretical input impedance of the Transfer Matrix Model and the measurements of a gaita hembra with 4 toneholes closed.
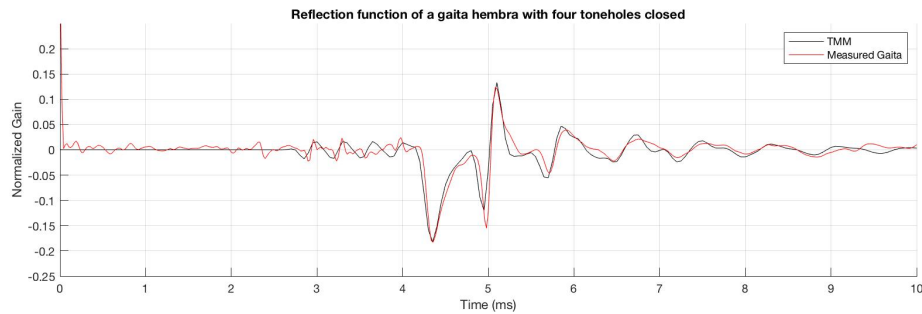
Fig. 4.6   Comparison between the theoretical reflection function of the Transfer Matrix Model and the measurements of a gaita hembra with 4 toneholes closed.

The case of three toneholes closed still shows a close correspondence with the theoretical model. We still see an amplitude difference in the fundamental peak. The theoretical model also shows peaks of slightly higher frequency than the measurements in the range 2-3 kHz. The reflection function also shows a close correspondence to the theoretical model.

The case with two toneholes closed is similar to the previous case, with three toneholes closed. The impedance measurements show a strong correspondence to the theoretical
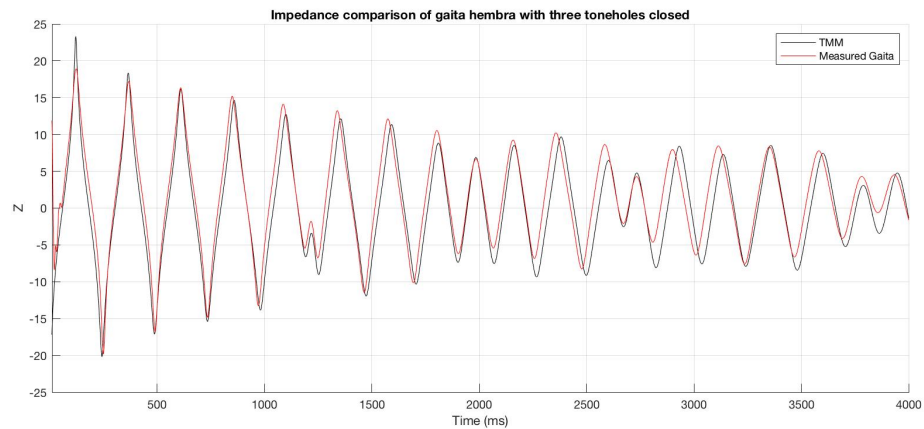
Fig. 4.7 Comparison between the theoretical input impedance of the Transfer Matrix Model and the measurements of a gaita hembra with three toneholes closed.
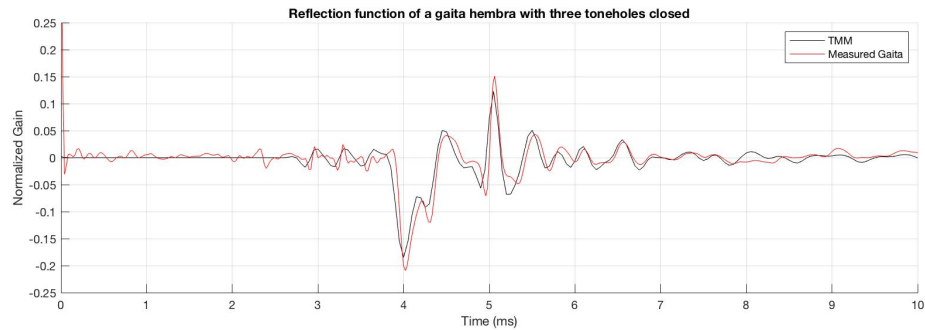
Fig. 4.8 Comparison between the theoretical reflection function of the Transfer Matrix Model and the measurements of a gaita hembra with three toneholes closed.

model, with some differences in the amplitude of the peaks, mostly in the fundamental. The modes of the theoretical model are slightly higher in frequency above 1.5kHz. The reflection shows the same behavior as the previous cases. The end reflection of the measurements is slightly stronger than the theoretical model.
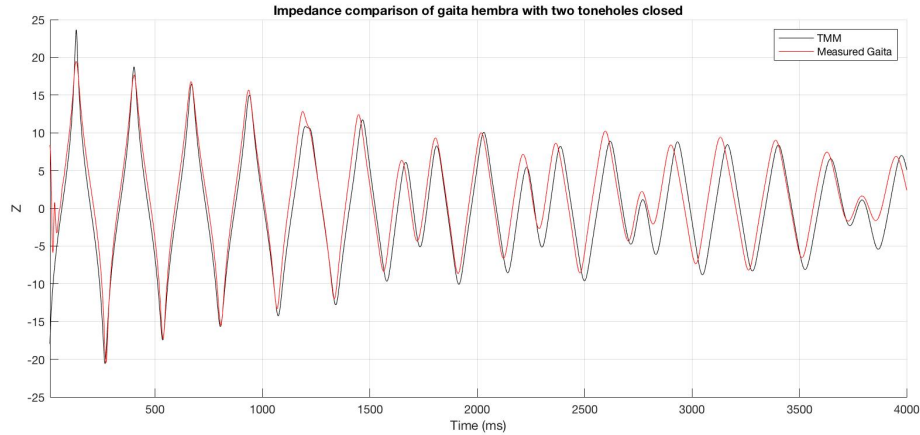
Fig. 4.9 Comparison between the theoretical input impedance of the Transfer Matrix Model and the measurements of a gaita hembra with two toneholes closed.
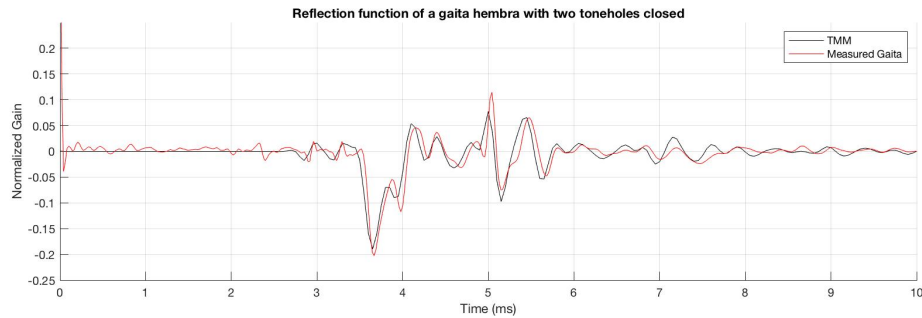
Fig. 4.10 Comparison between the theoretical reflection function of the Transfer Matrix Model and the measurements of a gaita hembra with two toneholes closed.

The case of a gaita hembra with one tonehole closed shows once again a similar behavior to the previous configuration. The impedance measurements show a strong correspondence. The fundamental of the theoretical model is 4dB higher than the measurements, and the modes above 1.5kHz are slightly higher in frequency. The reflection function shows a similar behavior than in previous cases.

The case with all toneholes open shows a strong correspondence in the impedance, with
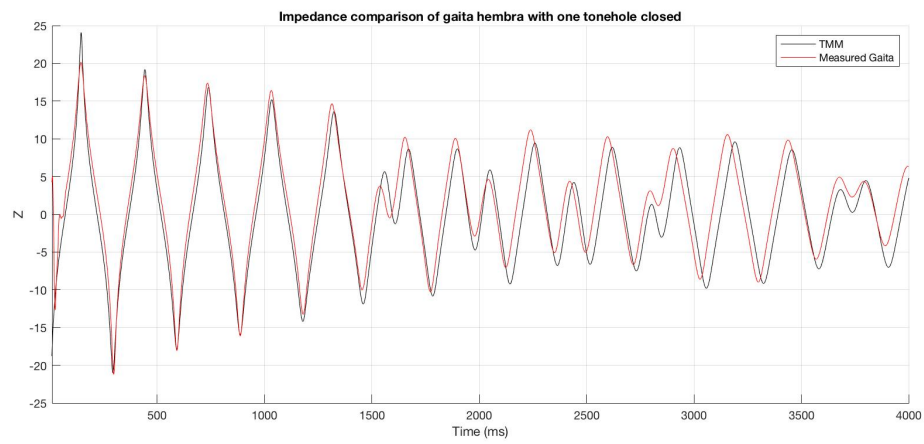
Fig. 4.11 Comparison between the theoretical input impedance of the Transfer Matrix Model and the measurements of a gaita hembra with one tonehole closed.
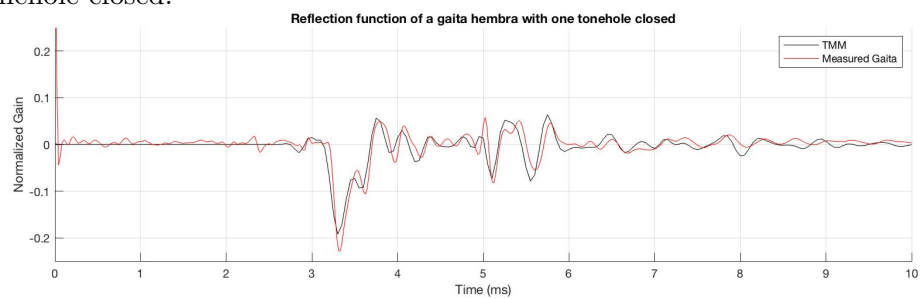
Fig. 4.12 Comparison between the theoretical reflection function of the Transfer Matrix Model and the measurements of a gaita hembra with one tonehole closed.

some difference in the amplitude of the peaks, as well as a strong correspondence in the reflection function. The first impedance peak shows an amplitude difference of 5dB. The reflection from the first open hole is aligned for both at 3ms, and subsequent reflections also correspond.
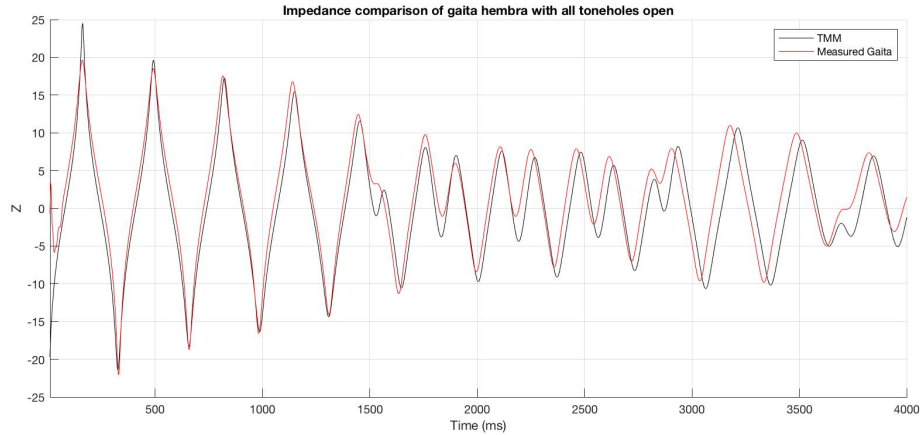
Fig. 4.13   Comparison between the theoretical input impedance of the Transfer Matrix Model and the measurements of a gaita hembra with all toneholes open.
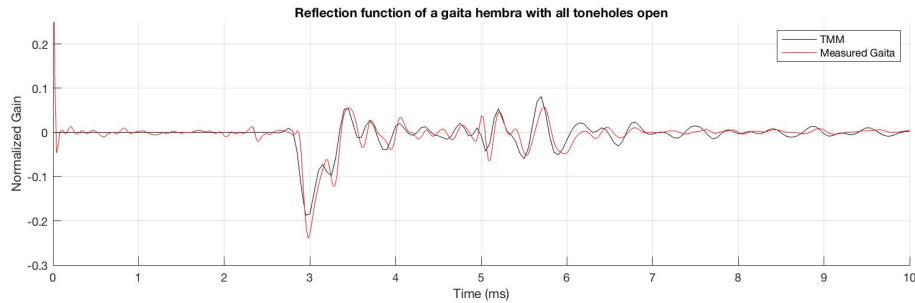
Fig. 4.14   Comparison between the theoretical reflection function of the Transfer Matrix Model and the measurements of a gaita hembra with all toneholes open.

In general, the impedance of the transfer matrix model corresponds to the measured impedance of the instrument, with small differences in frequency. The amplitude of the first peak of the model is 4-5dB higher than the measurements in all the measurements, and the amplitude of the resonances tends to decay faster and more steadily in the transfer matrix model. Resonances in the model are slightly higher than the measurements in the range above 2kHz. The reflection function shows strong correspondence with the theoretical

model. Some slight differences in the end reflection can be observed.

4.4.2 Gaita Macho

Three tonehole state configurations were measured for the gaita macho. Results were expected to be quite similar, as in theory, the only difference between the two instruments is the number of toneholes. The first case is the gaita macho with both toneholes closed. The impedance measurements show some significant discrepancies in amplitude of most peaks, except for the first one, and a strong correspondence in frequency. The reflection function shows a strong correspondence, with the reflection from the open end differing by 0.05ms.
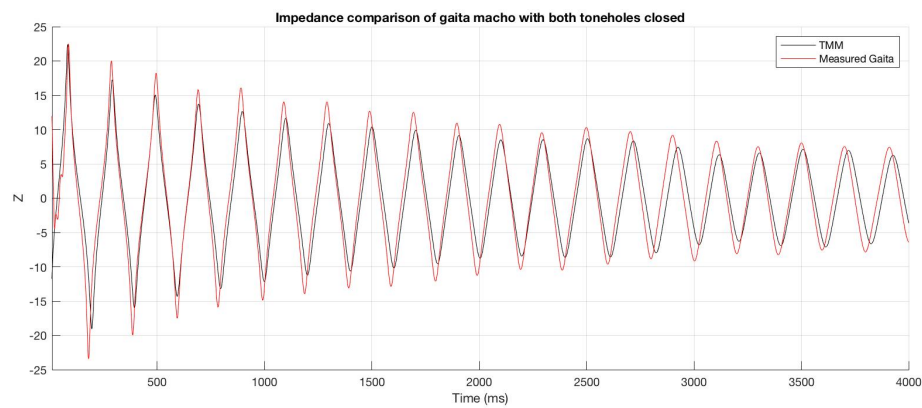
Fig. 4.15   Comparison between the theoretical input impedance of the Transfer Matrix Model and the measurements of a gaita macho with both toneholes closed.
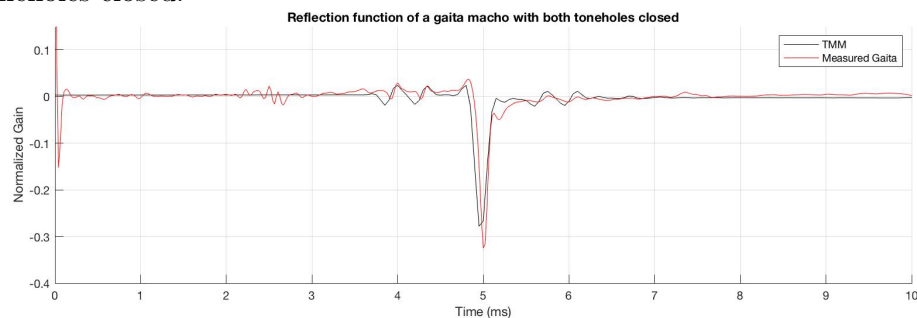
Fig. 4.16   Comparison between the theoretical reflection function of the Transfer Matrix Model and the measurements of a gaita macho with both toneholes closed.

The next case is the gaita macho with one tonehole closed, where the impedance measurements show a similar behavior to the previous case: there is a strong correspondence in frequency, with some discrepancies in amplitude, although not as significant as in the previous case. The reflection function also shows a strong correspondence, with the reflection from the open tonehole differing by 0.025ms. The measured reflection function of the instrument shows a stronger reflection from the open end than the theoretical model.
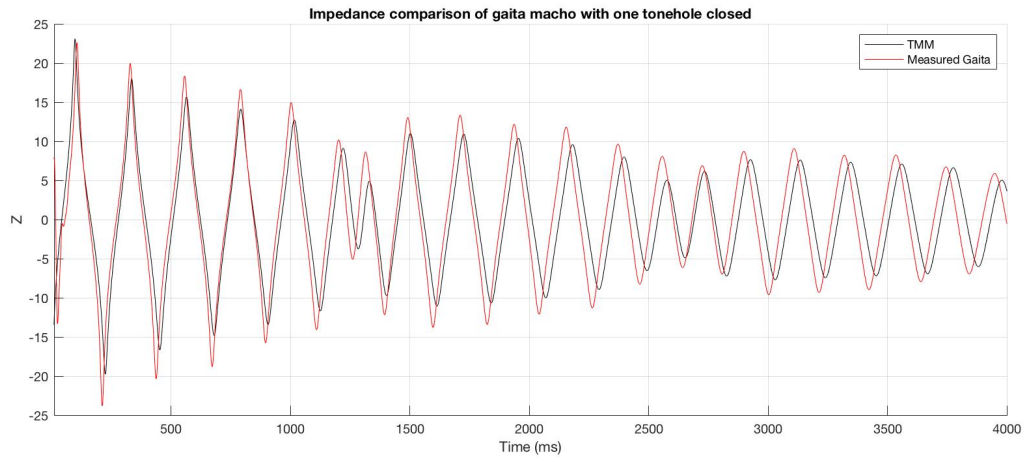
Fig. 4.17   Comparison between the theoretical input impedance of the Transfer Matrix Model and the measurements of a gaita macho with one tonehole closed.
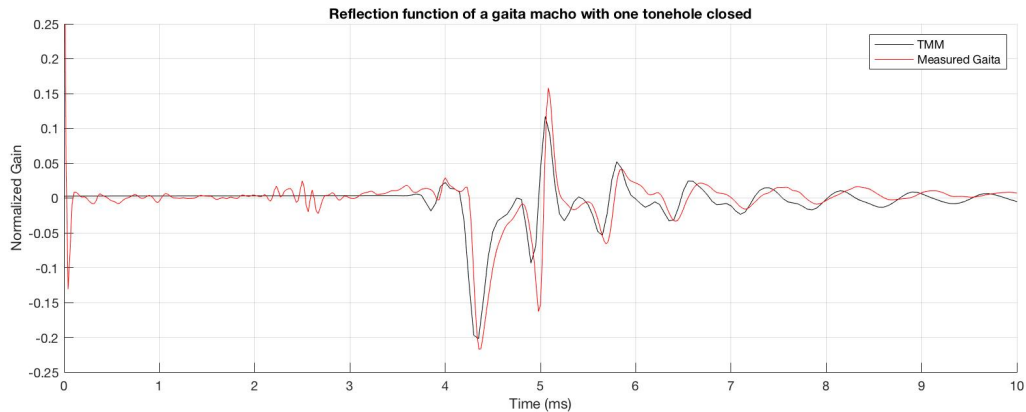
Fig. 4.18   Comparison between the theoretical reflection function of the Transfer Matrix Model and the measurements of a gaita macho with one tonehole closed.

The last case is the gaita macho with both toneholes open. This configuration of

tonehole states shows a difference of 7dB in the amplitude of the first peak. Subsequent peaks correspond with the model in terms of amplitude. Resonant peaks over 1kHz are 20-50Hz higher in frequency in the theoretical model. The reflection function shows a strong correspondence, with the reflection from the first open hole differing by 0.05ms. Once again, the measurements show a stronger reflection from the open end than the theoretical model.
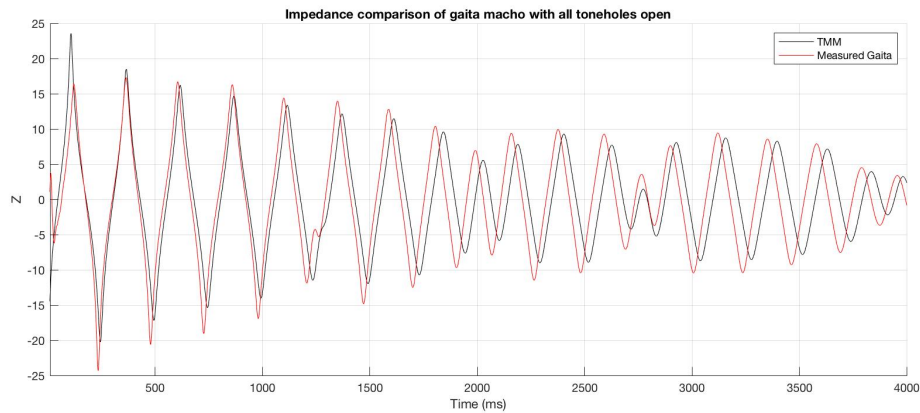
Fig. 4.19 Comparison between the theoretical input impedance of the Transfer Matrix Model and the measurements of a gaita macho with both toneholes open.
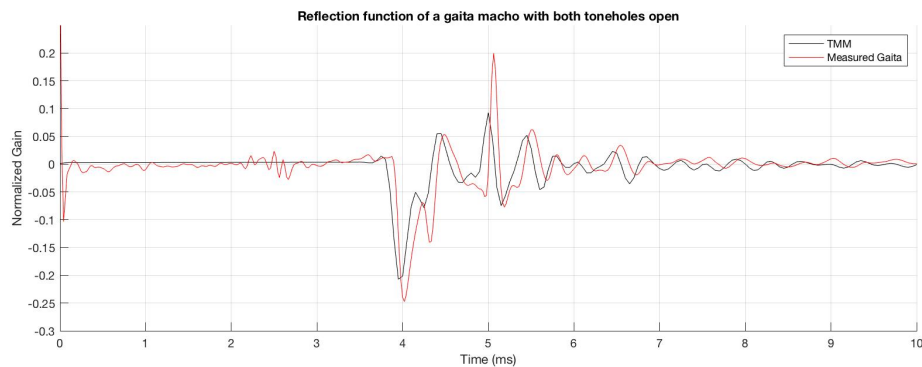
Fig. 4.20 Comparison between the theoretical reflection function of the Transfer Matrix Model and the measurements of a gaita macho with both toneholes open.

The reflection function of all three tonehole state configurations of the gaita macho show a strong correspondence between the theoretical model and the measurements taken from the instrument. The impedance measurements, however, show a significant difference

in the amplitude of the frequency peaks, particularly the first one, which is likely due to a slight leak when connecting the gaita to the measurement probe. The reflection function shows a strong correspondence with the theoretical model.

4.5 Conclusion

After comparing the results of the transfer matrix model with the measurements taken from a pair of instruments, a cylindrical model seems like a reasonable approximation, in spite of the slightly conical geometry of the instrument. The radius of the toneholes and the modeled speed of sound were modified slightly in the theoretical model in order to better approximate the response of the measurements. The impedance and reflection function of both instruments seem to be closely related to the theoretical response, with some differences mainly in the amplitude of the resonances. The configurations with all toneholes closed seem to be better aligned with the theoretical response. In configurations with at least one tonehole open, the reflection from the open end of the instruments is stronger than that of the theoretical model, which suggests that a refinement to the end reflection filter might be needed.

Chapter 5

Implementation of the Gaita Model

The implementation of the gaita model was done in two steps. First, it was written in *MATLAB* for visualizing the impedance and reflection function data, testing and debugging. Once the *MATLAB* model was running, the model was implemented in real-time using *JUCE* [48] and the *Synthesis ToolkKit* [9]. Figure 5.1 shows a block diagram of the implementation of a gaita with two toneholes. The implementation with five toneholes follows the same principle, with additional delay lines and three-port scattering junctions.
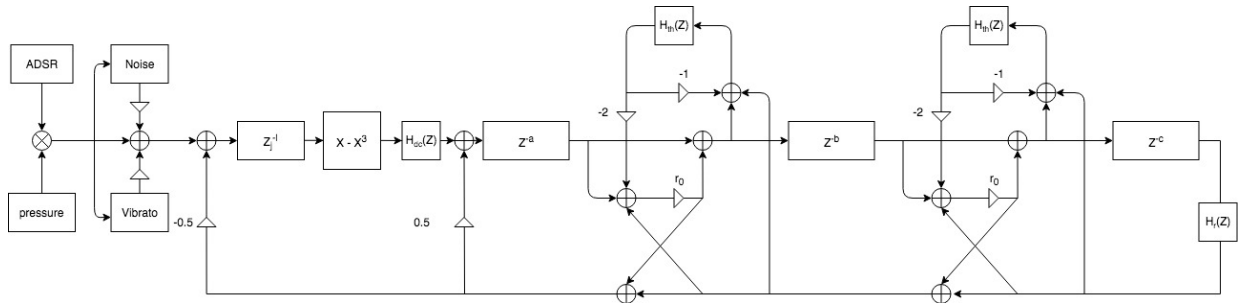
Fig. 5.1 Diagram of the implementation of the model with two toneholes, using the polynomial excitation model.

This model makes use of the components previously discussed in Chapter 3. The linear element of the model is composed of $n + 1$ integer delay lines, connected by n three-port scattering junctions, where n is the number of toneholes implemented in the model. The three-port scattering junction is simplified to use a single delay line per tube section, as shown in Fig. 5.2. The length of each delay section, a, b, etc. is determined by $d_i = \frac{2L}{cT}$, where L is the length of the section, c is the speed of sound and T is the sampling period.

The effective length of the air column thus depends on the tonehole states: it is the distance from the input end of the acoustic tube to the first open hole. If no holes are open, the length of the air column is equal to the length of the acoustic tube.
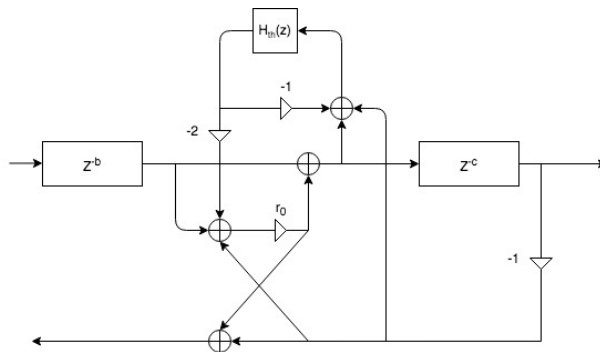
Fig. 5.2 Simplified three-port scattering junction using a single delay line per tube section.

The air jet mechanism uses the simple mechanism shown and explained in Section 3.2.4 and shown in Fig. 3.14 using a variable interpolating delay line. The length of this delay line, l, is a fraction of the air column delay, varying from 0.08 and 0.56 times the air column delay length. The model keeps track of the states of the toneholes in order to set the length of the jet delay line appropriately.

A first-order IIR filter was used to implement the reflection filter for simplicity of the model. Figure 5.3 shows the magnitude and phase response of three alternative filters: a filter designed using *openpipe.m* from [7], for an unflanged cylindrical pipe of radius 7.45mm, using a sample rate of 44.1 kHz, the filter proposed in [13] for a model of a gaita hembra, and a filter based on the STK flute model. A DC block filter is used after the non-linearity to remove the DC component that builds up from signal circulating in the delay line loop [6]. The pressure input of the model is shaped using an ADSR envelope. Noise and vibrato are also added to the input of the instrument.

5.1 MATLAB Implementation

The MATLAB implementation of the gaita model was used to visualize the impedance response and reflection function of the linear element of the digital waveguide model and compare the results to the measurements and the transfer matrix model discussed in Chap-

ter [4]. The end reflection filter used was the filter designed using *openpipe.m*, shown in Fig. 5.3.
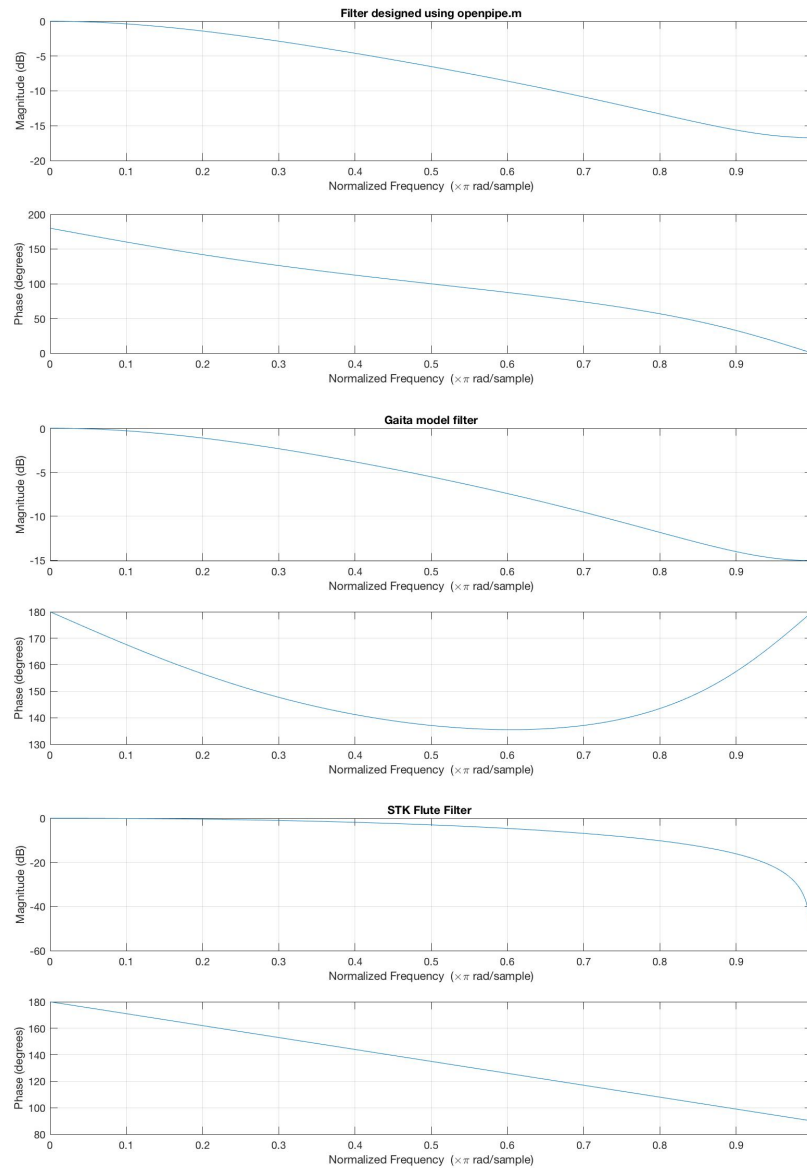
Fig. 5.3   Frequency and phase response of end reflection filters, from top to bottom: filter designed using *openpipe.m* from [7], filter proposed in [13] for a gaita model, filter based on STK Flute.

Figure 5.4 shows the measurements of the reflection function of the gaita hembra, along with the corresponding transmission matrix and digital waveguide model results in all state

configurations.

Reflection function of a gaita hembra with all toneholes closed

Reflection function of a gaita hembra with four toneholes closed

Reflection function of a gaita hembra with three toneholes closed
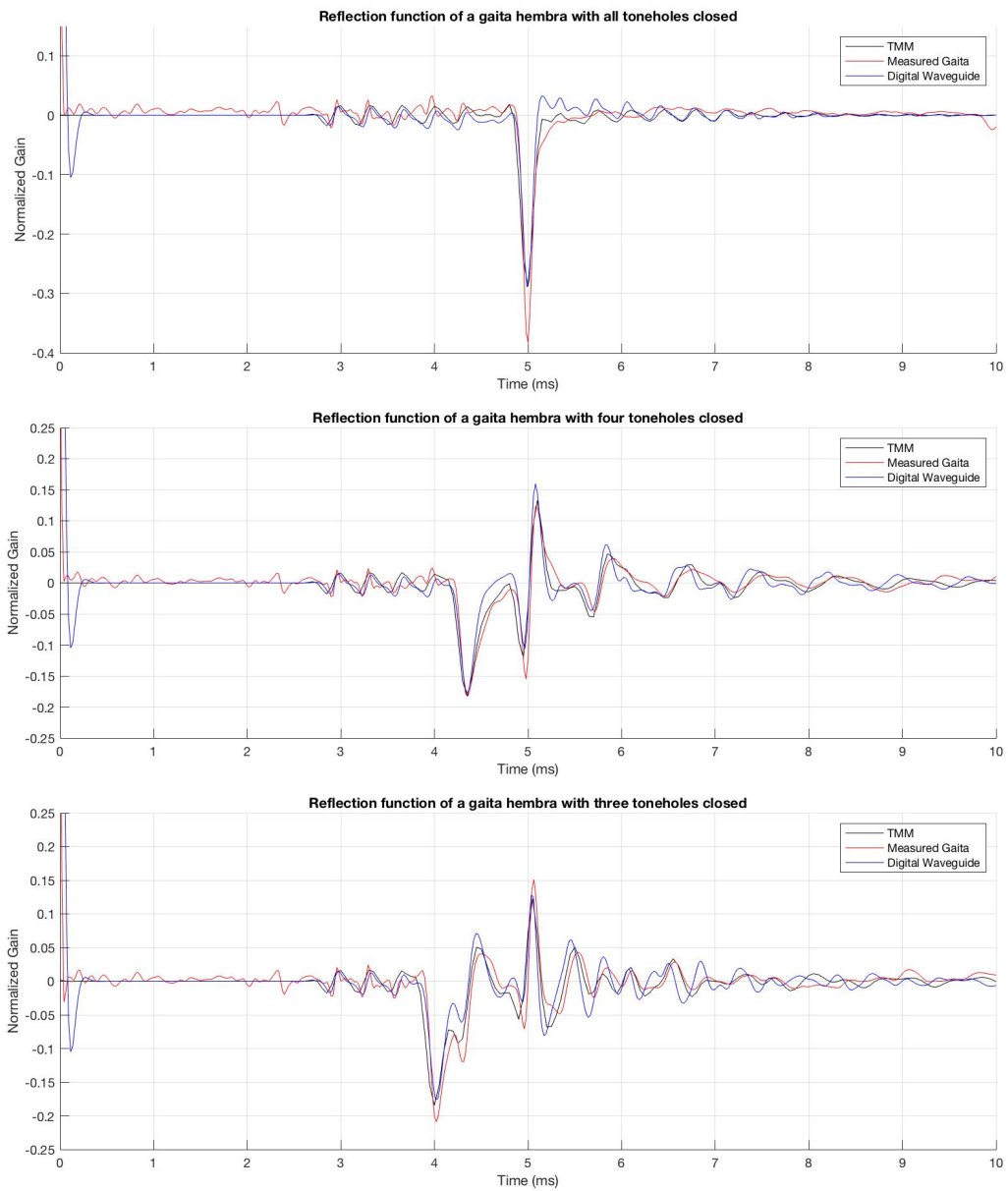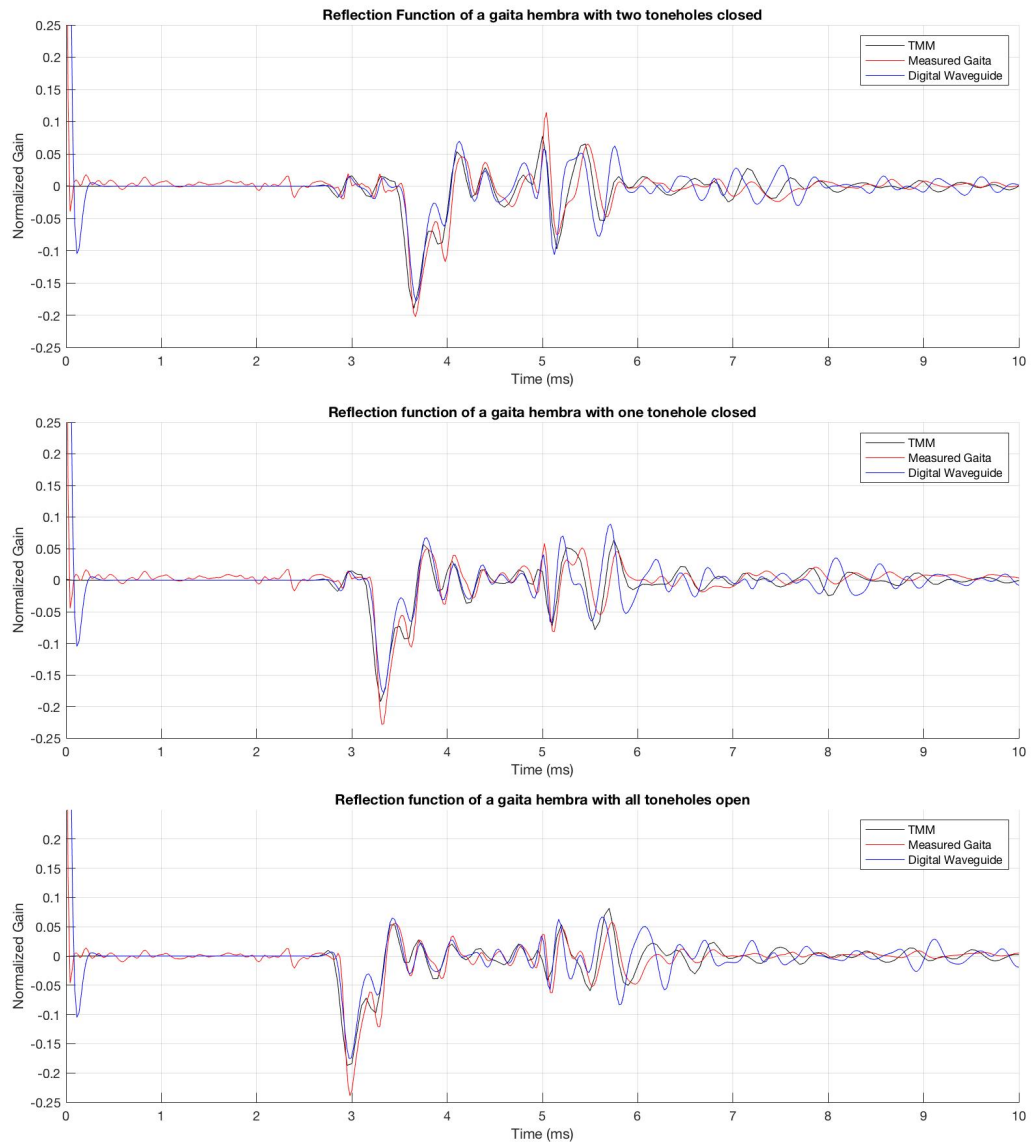
Fig. 5.4   Comparison of the reflection function of the digital waveguide
model of the gaita hembra in all tonehole state configurations from all closed
(top) to all open (bottom).

Figure 5.5 show the same comparison in the case of a gaita macho. The results for the
gaita hembra show that the reflection function of the digital waveguide model has a strong
correspondence with the theoretical model and the measurements from the instrument.
Some discrepancies can be observed after the end reflection, which may be caused by the

use of integer delay lines in the model. The results from the gaita macho show that the measurements have a stronger reflection from the open end, particularly in the configuration with both toneholes open.
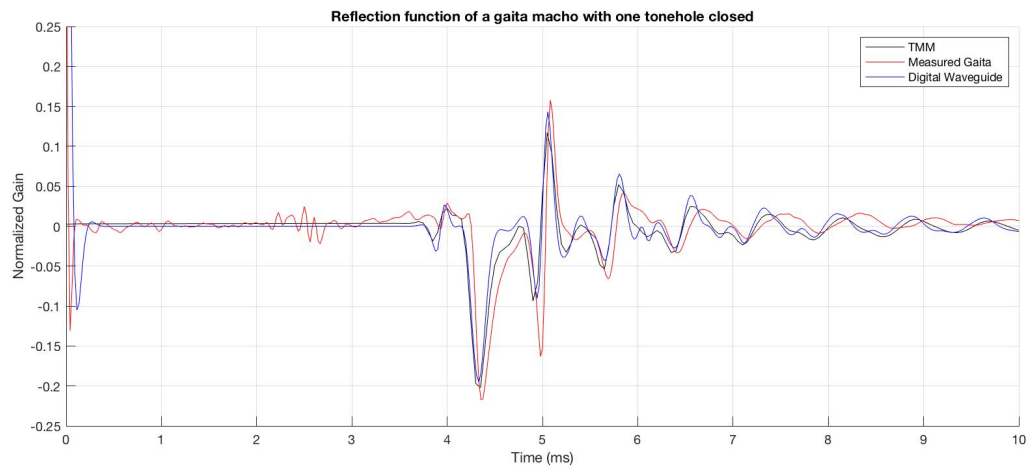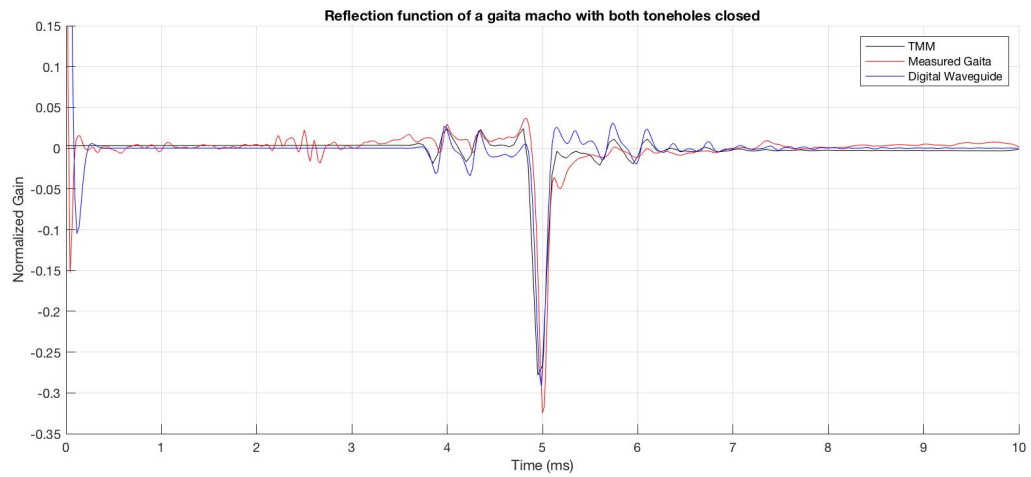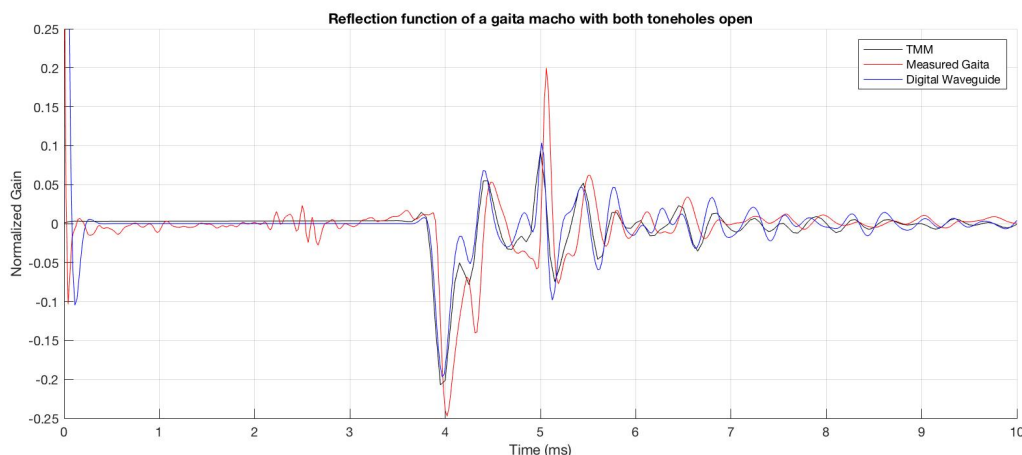
Fig. 5.5 Comparison of the reflection function of the digital waveguide model of the gaita macho in all tonehole state configurations from all closed (top) to all open (bottom).

5.2 Real-Time Implementation

While *MATLAB* offers a great tool for prototyping, debugging and visualizing data, it becomes limiting when there is a need to test and update different parameters and compute the output in real time. A real-time implementation was created for this purpose using the JUCE framework and the STK.

5.2.1 The JUCE Framework

JUCE is a partially open source, cross-platform C++ application framework [48] used for the development of multimedia applications, including VST, Audio Units and AAX audio plugins, as well as standalone applications. Educational and personal licenses for JUCE are free. JUCE offers a variety of modules to handle GUI elements, audio, MIDI, and more. The *Projucer* application, included with the download of JUCE, is used to include all the necessary modules into the project and link external libraries. It exports the project to the native IDE of the system with all the necessary preprocessor definitions and compiler flags. This implementation used JUCE 5.4.5 and Xcode 7.3.1. JUCE modules were used to create a GUI with buttons, sliders and check box controls. JUCE also handles the audio engine of the application.

5.2.2 The STK

The Synthesis ToolKit is a set of open source C++ classes for audio signal processing and algorithmic synthesis [9]. The STK classes make it easy to implement a model such as the one presented in this project, as it includes classes for all of the particular elements of the model, including delay lines, filters, envelopes and generators. It also includes examples of physical models and programs that can be used as a starting point for the implementation of new programs. A few example instrument models included in the STK were useful in the development of this model, including Flute, BlowHole and Recorder.

5.3 The application

The application consists of a simple GUI with slider controls for the parameters of the physical model, as shown in Fig. 5.6. Controls for the application are shown in Table 5.1. The application is available for download from this link.

5.4 Comparison

In order to compare the model and the real instrument, some recordings of a gaita were made, in different tonehole state configurations playing the first harmonic of the position. The recordings were made using an AKG C214 condenser microphone through a Universal Audio 4-710d preamplifier, using a close microphone technique in a room without acoustic treatment. These recordings are compared with the output of the application. Configurations with four toneholes closed and all toneholes open are shown. The noise gain and the jet ratio were adjusted to best match the note tunings. The spectrogram was computed using a 1024 sample FFT with 512 samples of overlap.

The comparison of the frequency spectra and the spectograms of different configurations of tonehole states shows some commonalities. One general and noticeable difference between the model and the real instrument is in their spectral envelopes. The model produces a fundamental note with several distinct harmonic peaks. Figure 5.7 shows the largest discrepancy: while the recording of the first position of the gaita hembra shows only five or six distinct peaks and no significant peaks higher than 3 kHz, the model shows distinct peaks going up around 8kHz.

On-screen keyboard	On-screen MIDI Keyboard
Note On/Off	Start and end a note
Excitation model selection menu	Drop-down menu to choose between the polynomial excitation model (STK Flute) and the recorder model by Verge et al. (STK Recorder)
Gain	Output gain of the application
Blow Pressure	Blow pressure value when using the recorder model (unavailable for the flute excitation model)
Vibrato Frequency	Frequency of the sine wave controlling the vibrato of the model
Vibrato gain	Amplitude of the sine wave controlling the vibrato of the model
Noise gain	Amplitude of the noise component at the input of the model
Breath Cutoff	Cutoff frequency of the turbulence filter in the recorder model (unavailable for the flute excitation model)
Jet Ratio	Changes the length of the jet delay line in proportion to the effective length of the air column, given the tonehole state configuration (unavailable in the recorder excitation model)
Hole	State of the tonehole: A checked box is a closed tonehole. An empty box is an open tonehole.
Softness	Softness parameter for the recorder model, explained in [12] (Unavailable in the flute excitation model)

Table 5.1   Parameters available for the real-time control of the model.
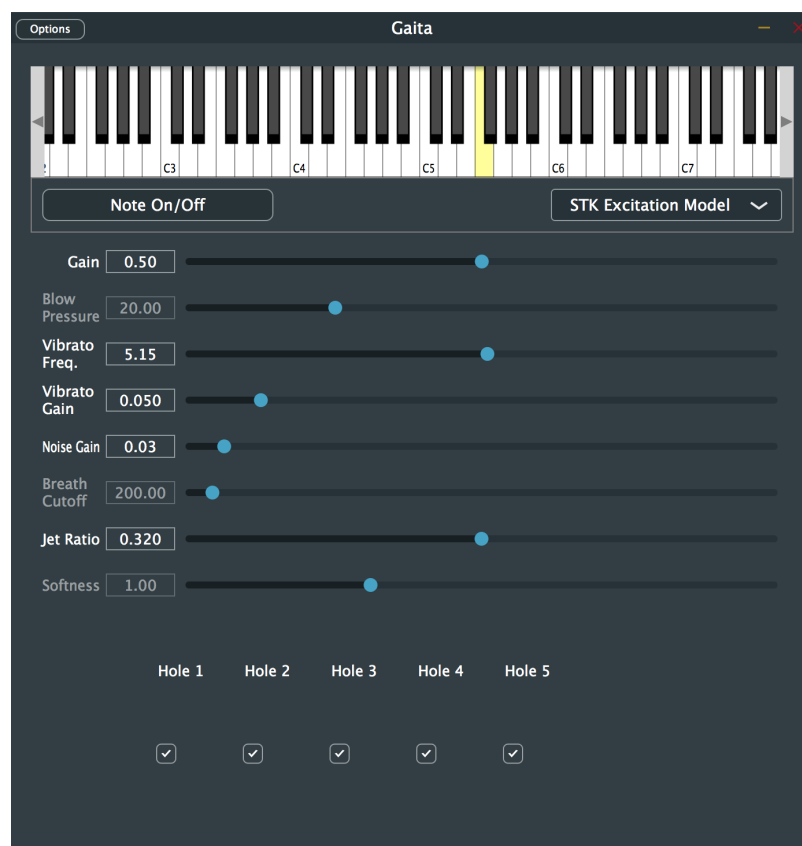
Fig. 5.6 Screenshot of the gaita application.

The model also shows a significant presence of the overtones of the fundamental note of the instrument in each position, and while the recordings of the instrument do show some peaks corresponding to these overtones, their amplitude relative to the overtones of the note played is significantly lower.

From the visualization and the audio of the recordings, an obvious characteristic of the instrument is its noise. In general, the instrument has a significant noise component. While the model does integrate noise and allows the user to control the gain of the noise, it is clear that the spectro-temporal characteristic of the noise component of the instrument are different from those of the model. The noise component of the model is created using the Noise.h class in the STK and is subject to some low-pass filtering. The decay of this noise component is linear, while the frequency spectra of the recordings show a certain degree of randomness in the decay of the noise. Looking at the spectrograms, we can see that the model has more energy in the high range of the frequency spectrum than the instrument.
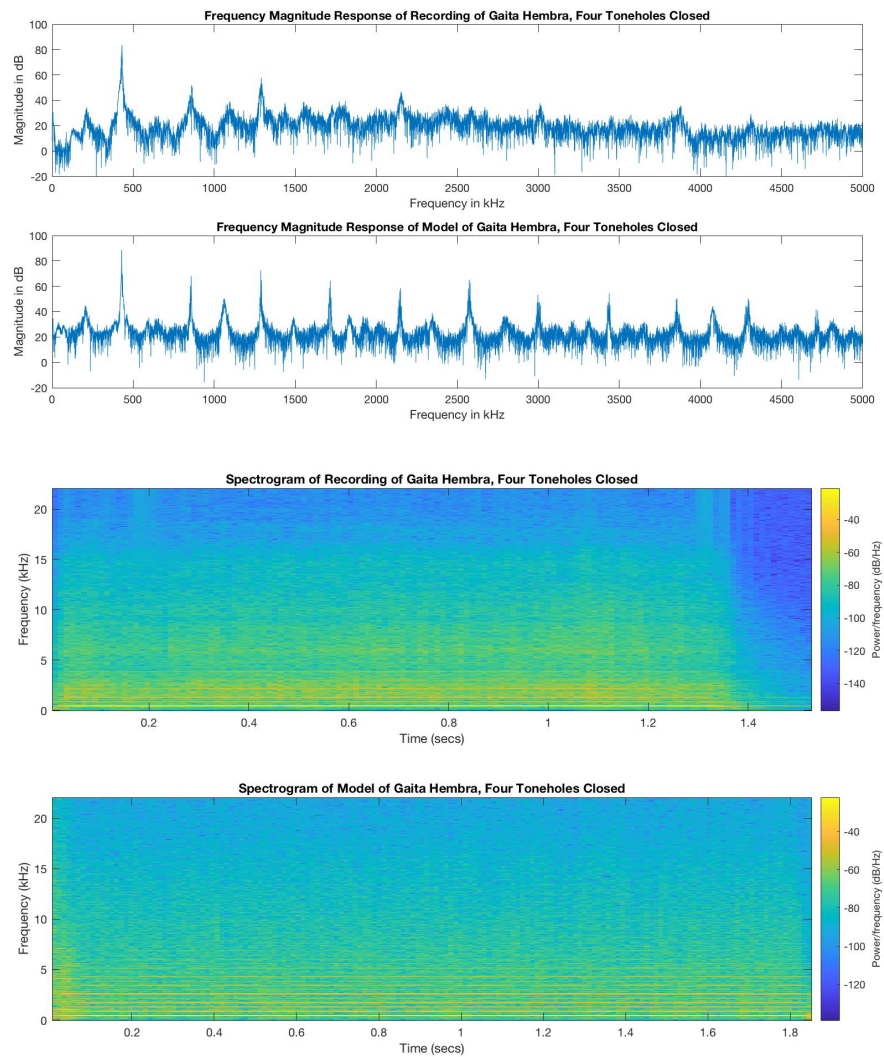
Fig. 5.7 Frequency magnitude response and spectrogram of the model and recording of a gaita hembra with four toneholes closed.
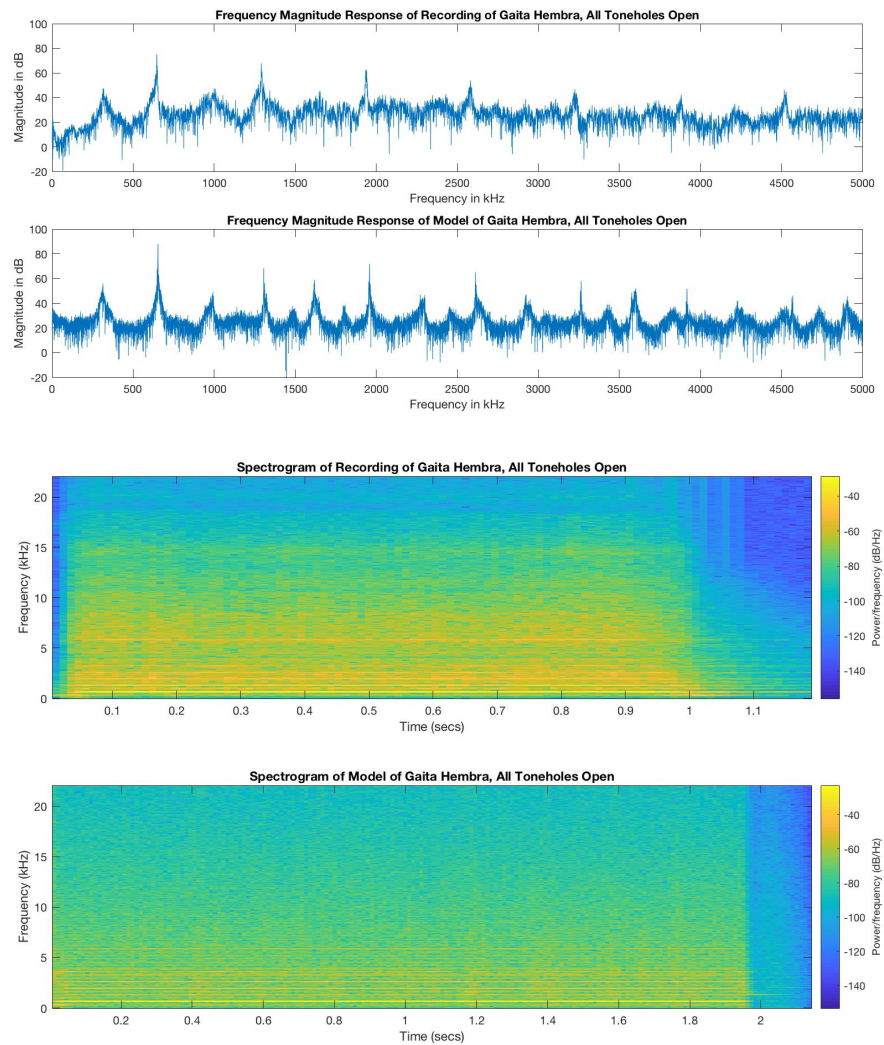
Fig. 5.8 Frequency magnitude response and spectrogram of the model and recording of a gaita hembra with all toneholes open.

We can also notice a difference in the temporal aspect of the high frequency energy. In the model, the whole frequency spectrum has the same envelope. In the recordings, the high-frequency components of the sound show a slightly longer attack and decay times than the lower portion of the frequency spectrum.

The discrepancies between the modeled and recorded sounds shown above are not surprising, as the output from the model corresponds to a pressure pickup located inside the air column of the instrument. In order to more fairly compare the results, the internal pressure was highpass filtered using the filter shown in Fig. 5.9 to simulate the effect of sound radiation from a tonehole lattice. At the same time, the presence of much more high-frequency content in modeled results of Figs. 5.7 and 5.8 indicated that the open-end filter needed to be revised, with a lower lowpass filter cutoff frequency. Thus, the open-end filter was changed to the characteristic also shown in Fig. 5.9.
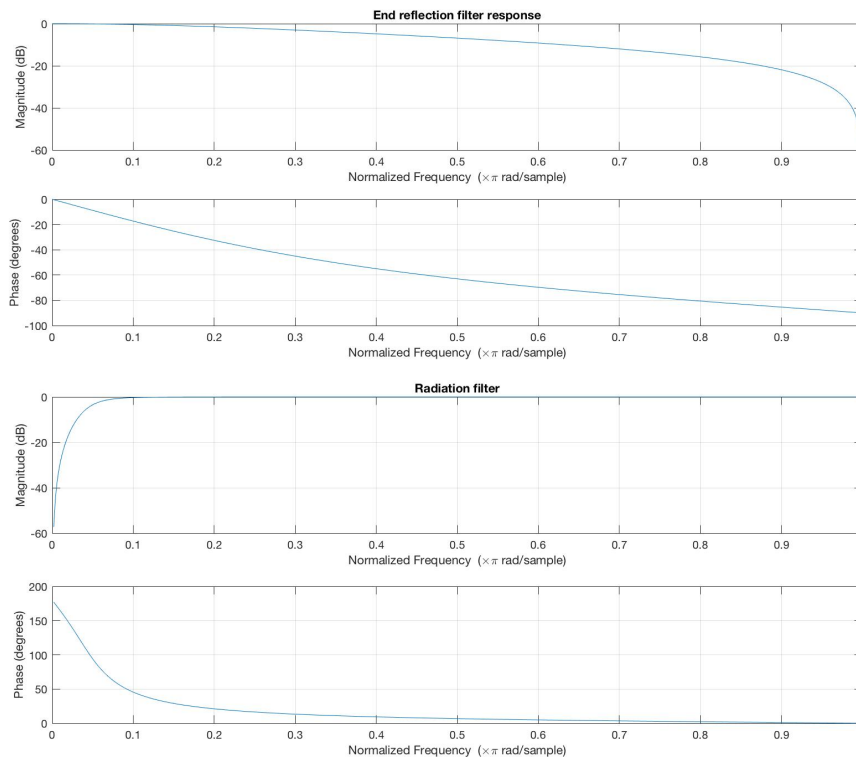
Fig. 5.9   Magnitude and phase response of the end reflection and radiation filters of the model.

Figures 5.10 and 5.11 show the frequency magnitude response and spectrogram comparisons of the model of the gaita hembra with four toneholes closed and all toneholes open

playing the second harmonic. These results show improvement in the relationship between the magnitude of the harmonic peaks, particularly in the case of four toneholes open.
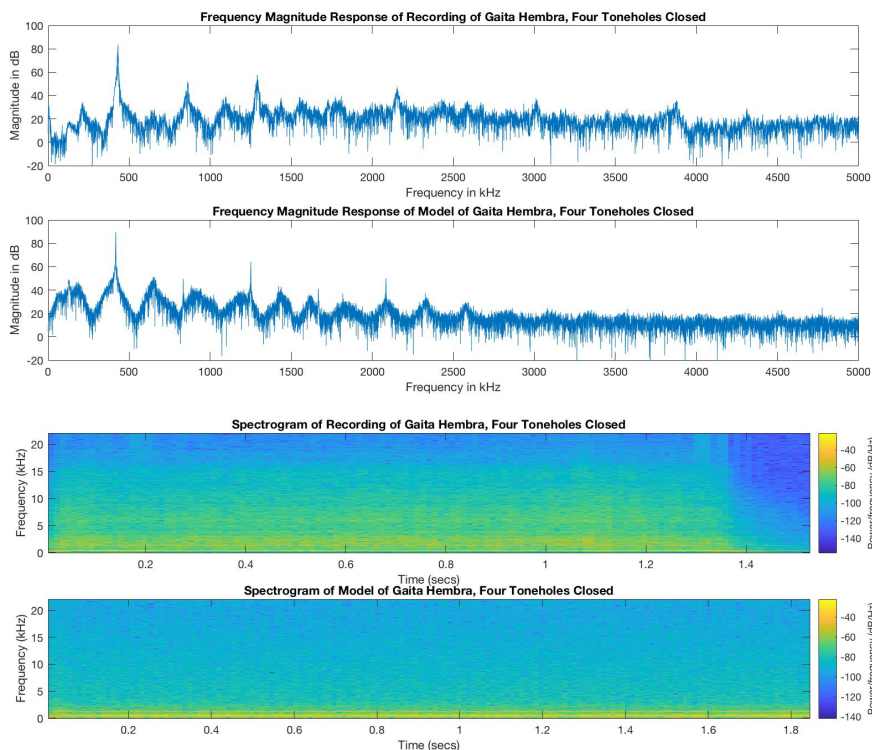
Fig. 5.10   Frequency magnitude response and spectrogram of the model using the modified filter and recording of a gaita hembra with four toneholes closed.

Figure 5.12 shows the frequency magnitude response of a recording of the model using the recorder excitation mechanism. The frequency magnitude does not seem to correspond very well to that of the recording of the instrument. The recorder model is much more sensitive to adjustments in the parameters, and a careful adjustment may yield improve results.
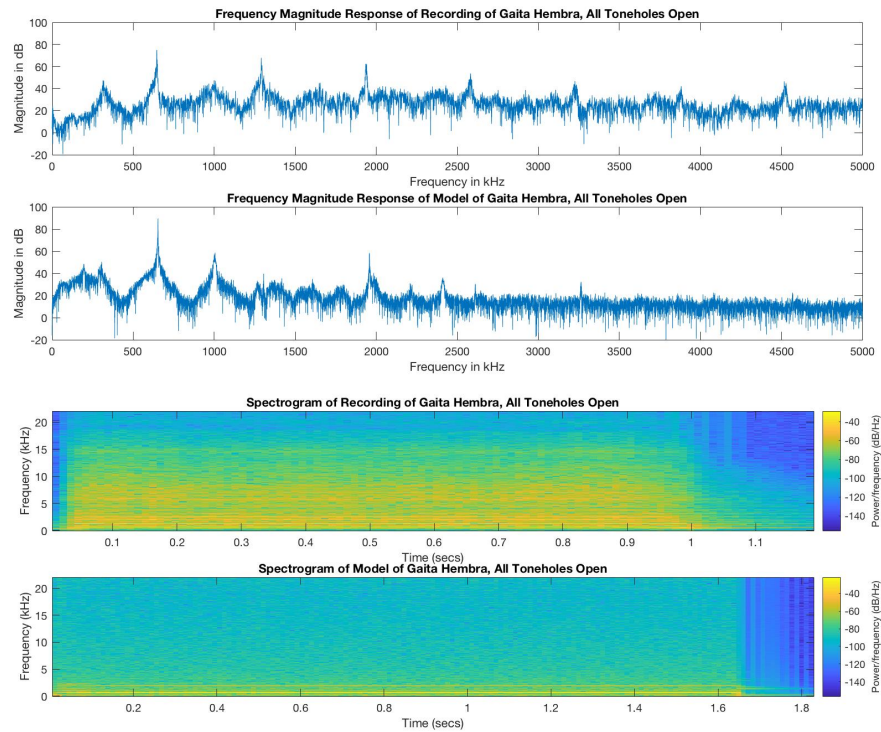
Fig. 5.11 Frequency magnitude response and spectrogram of the model using the modified filter and recording of a gaita hembra with all toneholes open.
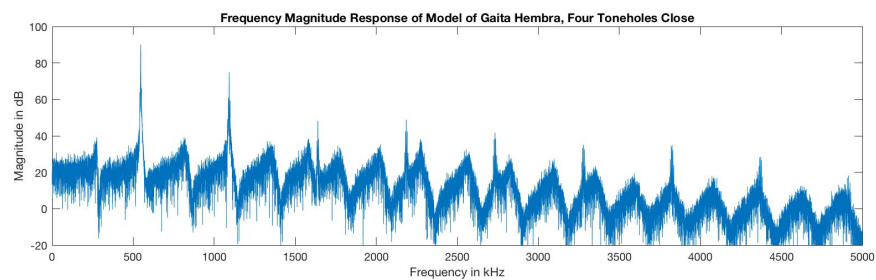
Fig. 5.12 Frequency magnitude response and of the model a gaita hembra, using the recorder model with four toneholes closed.

Chapter 6

Conclusion

This project intended to develop and implement a physical model of a gaita, a traditional Colombian wind instrument. Basic acoustic principles were reviewed, as well as acoustical aspects of wind instruments in order to understand the behavior of the instrument. Digital waveguide modeling techniques were reviewed and explained in order to implement and test the model. The development of the model was informed by physical measurements of the impedance response of the acoustic tube of a pair of instruments, after their heads were removed, and the measurements were compared with theoretical models for cylindrical tubes with toneholes and measurements of the digital waveguide implementation. The linear element of the digital waveguide model developed seems to be a close approximation to the response of the acoustic tube of the real instrument, but the synthesized sound fails to accurately model some characteristics of the instrument, in particular those related to noise in the sound. The model was implemented for real-time synthesis using JUCE and the STK, and includes a user-friendly graphical interface, offering control of different parameters. Recordings of the instrument were made in order to compare the frequency response and spectrograms of the recordings and the synthesized sound.

6.1 Limitations and further work

Due to the artisanal nature of the instrument, it is quite possible that the response of different instruments made by different instrument makers have significant differences in their response. The analysis in this study is therefore limited to the particular pair of gaitas used. A more in-depth study would perform measurements on several different instruments

and average the response for a more general model.

The model is fairly simple and the implementation fails to accurately reproduce some of the characteristics of the gaita. The relative amplitudes of the harmonic components of the instrument are not an accurate representation of the instrument. The model outputs the pressure at the mouthpiece, and although the end reflection filter induces some losses, losses due to radiation from the end and from the toneholes are not fully taken into account. In order to improve on this, the radiation filter, with a cutoff frequency corresponding to that of the instrument's tonehole lattice was added to the output of the instrument. The results after the filter was added showed some improvement in some cases, but a more accurate model for radiation losses could further improve the results.

The noise component of the instruments is a characteristic feature of its sound, and the model fails to capture the noise profile of the instrument. The recorder excitation model could potentially improve on the noise profile with a careful adjustment of the parameters of the model. The model is also at an experimental stage, where the user can modify parameters in real-time, but it is not a playable instrument. In order to render the model into a playable instrument, a careful adjustment of certain parameters is needed. The application can save and load the state of the parameters, which can be helpful to create a mapping of the parameters to MIDI notes.

Some ideas for the refinement of the model can also include the implementation of a separate noise component that captures the spectral envelope of the instrument's noise more accurately. The placement of the toneholes along the acoustic tube could be a user controlled parameter in order to adjust the tuning of the instrument.

Appendix A

Gaita Code

```cpp
GaitaH :: GaitaH(int nToneholes, int* delayLengths, StkFloat* toneholeRadii)
{

    nToneholes_ = nToneholes;
    toneholeRadii_ = toneholeRadii;
    int i;
    radius_ = 0.00745;

    vibrato_.setFrequency( 5.925 );
    filter_.setCoefficients(0.3375, 0.3375, -0.3249)
    noiseFilter_.setCoefficients( 0.161328, 0., -0.161328, -1.555063, 0.620405);
    radiationFilter_.setCoefficients( 0.8897, -1.7794, 0.8897, -1.7672, 0.7916);
    dcBlock_.setBlockZero();

    adsr_.setAllTimes( 0.005, 0.01, 0.8, 0.010 );
    endReflection_ = 0.5;
    jetReflection_ = 0.5;
    noiseGain_     = 0.15;    // Breath pressure random component
    vibratoGain_   = 0.05;    // Breath periodic vibrato component
    jetRatio_      = 0.32;

    boreDelay_ = (DelayL *) new DelayL[nToneholes_+1];
     airColumnLengths_ = (int *) new int[nToneholes_+1];
     airColumnLengths[0] = 0;
```

```
    for (int i = 0; i <= nToneholes_; i++)
    {
    boreDelay_[i].setDelay(delayLengths[i])
    airColumnLengths[i] += delayLengths[i];
    }


    airColumnLengths_[0] = boreDelay_[0].getDelay();
    for (i = 1; i <= nToneholes_; i++)
    {
        airColumnLengths_[i] = airColumnLengths_[i-1]
                                 + boreDelay_[i].getDelay();
    }

    toneholes_ = (Tonehole *) new Tonehole[nToneholes_];
    scatter_ = (StkFloat *) new StkFloat[nToneholes_];

    char thState[] = "CLOSED";
    for (i = 0; i < nToneholes_; i++)
    {
        toneholes_[i].setRadius( toneholeRadii_[i] );
        toneholes_[i].setRate(0.01);
        scatter_[i] = -pow(toneholeRadii_[i], 2)
                        / ( pow(toneholeRadii_[i], 2) + 2
                        * pow(this->radius_, 2) );
        toneholes_[i].setState( thState );
    }

    this->setJetDelay(jetRatio_);
    this->clear();
}


StkFloat GaitaH :: tick( unsigned int )
{
    unsigned int i;
    StkFloat pressureDiff;
    StkFloat breathPressure;
    StkFloat samples[3], temp;
```

```
    // Calculate the breath pressure (envelope + noise + vibrato)
    breathPressure = maxPressure_ * adsr_.tick ();
    breathPressure += breathPressure *
                      ( noiseGain_ * noise_.tick () +
                        vibratoGain_ * vibrato_.tick ()  );

    // Calculate the differential pressure
    // = mouthpiece pressures − jet
    temp = boreDelay_ [0]. lastOut ();

    pressureDiff = breathPressure − (jetReflection_ * temp);
    pressureDiff = jetDelay_.tick ( pressureDiff );
    pressureDiff = dcBlock_.tick
                      ( jetTable_.tick ( pressureDiff ) )
                                    + (endReflection_ * temp);
    samples [0] = pressureDiff;
    p_mouth = samples [0];

    // Do three−port junction scattering for toneholes
    for (i=0; i<nToneholes_; i++) {
        samples [1] = boreDelay_ [i+1]. lastOut ();
        samples [2] = toneholes_ [i]. lastOut ();
        temp = scatter_ [i] *
                (samples [0] + samples [1] − 2 * samples [2]);
        toneholes_ [i]. tick (samples [0] + samples [1]
                            − samples [2] + temp);
        boreDelay_ [i]. tick (samples [1] + temp);
        samples [0] += temp;
    }

    // Do open−end filtering
    boreDelay_ [nJunctions_]. tick (filter_.tick (samples [0]) * −0.95 );
    p_mouth += 1.5 * boreDelay_ [0]. lastOut ();
    lastFrame_ [0] = 0.3 * radiationFilter_.tick (p_mouth) * outputGain_;
    lastFrame_ [0] += adsr_.lastOut () * 0.025 * outputFilter_.tick ( noise_.tick ());
    return lastFrame_ [0] ;
}
```

References

[1] F. Ochoa Escobar, *El libro de las gaitas largas: Tradición de los Montes de María*. Edtitorial Pontificia Universidad Javeriana, 2013.

[2] N. H. Fletcher and S. Thwaites, "The physics of organ pipes," *Scientific American*, vol. 248, no. 1, pp. 94–103, 1983.

[3] A. Chaigne and J. Kergomard, eds., *Acoustics of Musical Instruments*. 2016.

[4] M. E. McIntyre, R. T. Schumacher, and J. Woodhouse, "On the oscillations of musical instruments," *Journal of the Acoustical Society of America*, vol. 74, no. 5, pp. 1325–1345, 1983.

[5] G. P. Scavone, *Computational Modeling of Musical Acoustic Systems*. https://www.music.mcgill.ca/ gary/618/index.html, accesed November 2019.

[6] J. O. Smith, *Physical Audio Signal Processing*. http://ccrma.stanford.edu/~jos/pasp/, accessed September 2019. online book, 2010 edition.

[7] G. P. Scavone, *An acoustic analysis of single-reed woodwind instruments with an emphasis on design and performance issues and digital waveguide modeling techniques*. PhD thesis, Stanford University, 1997.

[8] G. P. Scavone and P. R. Cook, "Real-time computer modeling of woodwind instruments," in *Proceedings of the International Symposium on Musical Acoustics (ISMA-98)*, (Leavenworth,WA), pp. 197–202, 1998.

[9] P. R. Cook and G. P. Scavone, "The Synthesis ToolKit (STK)," in *International Computer Music Conference*, pp. 164–166, 1999.

[10] A. H. Benade, *Fundamentals of musical acoustics*. New York: Dover Publications, 1990.

[11] G. P. Scavone and P. R. Cook, "The Synthesis ToolKit in C++." https://ccrma.stanford.edu/software/stk/.

[12] M.-P. Verge, A. Hirschberg, and R. Caussé, "Sound production in recorderlike instruments. II. A simulation model," *The Journal of the Acoustical Society of America*, vol. 101, no. 5, pp. 2925–2939, 1997.

[13] D. Albarán, S. Aldana, and J. Villegas, "Síntesis de gaita hembra colombiana usando guías de onda digitales," in *Simposio de Tratamiento de Señales, Imágenes y Visión Artificial*, 2006.

[14] J. Montagu, *Origins and development of musical instruments*. Lanham, MD: Scarecrow Press, 2007.

[15] J. Hernandez Vega. Personal Communication, 2019.

[16] J. D. Hernandez, "Instrumental acoustics study of a gaita hembra,"

[17] J. W. Coltman, "Jet behavior in the flute," *The Journal of the Acoustical Society of America*, vol. 92, no. 1, pp. 74–83, 1992.

[18] P. De La Cuadra, *The sound of oscillating air jets: Physics, modeling and simulation in flute-like instruments.* PhD thesis, Stanford University, 2006.

[19] M.-P. Verge, B. Fabre, A. Hirschberg, and A. Wijnands, "Sound production in recorderlike instruments. I. Dimensionless amplitude of the internal acoustic field," *The Journal of the Acoustical Society of America*, vol. 101, no. 5, pp. 2914–2924, 1997.

[20] D. H. Keefe, *Woodwind tone hole acoustics and the spectrum transformation function.* PhD thesis, Case Western Reserve University, June 1981.

[21] D. H. Keefe, "Woodwind air column models," *The Journal of the Acoustical Society of America*, vol. 88, no. 1, pp. 35–51, 1990.

[22] N. Fletcher and L. Douglas, "Harmonic generation in organ pipes, recorders, and flutes," *The Journal of the Acoustical Society of America*, vol. 68, no. 3, pp. 767–771, 1980.

[23] A. Lefebvre and G. P. Scavone, "Characterization of woodwind instrument toneholes with the finite element method," *The Journal of the Acoustical Society of America*, vol. 131, no. 4, pp. 3153–3163, 2012.

[24] C. Nederveen, J. Jansen, and R. Van Hassel, "Corrections for woodwind tone-hole calculations," *Acta Acustica united with Acustica*, vol. 84, no. 5, pp. 957–966, 1998.

[25] J. O. Smith, "Musical applications of digital waveguides," technical report, Stanford University, 1987.

[26] J. O. Smith, "Physical modeling using digital waveguides," *Computer Music Journal*, vol. 16, no. 4, p. 74, 1992.

[27] V. Välimäki, B. Hernoux, J. Huopaniemi, and M. Karjalainen, "Measurement and analysis of acoustic tubes using signal processing techniques," in *Proc. Finnish Signal Processing Symposium*, 1995.

[28] P. R. Cook, "A meta-wind-instrument physical model, and a meta-controller for real-time performance control," *Proceedings of the International Computer Music Conference*, p. 273, 1992.

[29] V. Välimäki, M. Karjalainen, Z. Janosy, and U. K. Laine, "A real-time DSP implementation of a flute model," in *International Conference on Acoustics, Speech and Signal Processing*, pp. 249–252, 1992.

[30] V. Välimäki, R. Hänninen, and M. Karjalainen, "An improved digital waveguide model of flute-implementation issues," in *Proceedings of the International Computer Music Conference*, pp. 1–4, 1996.

[31] N. H. Fletcher and T. D. Rossing, *The physics of musical instruments.* New York: Springer, 2nd ed., 1998.

[32] C. J. Nederveen, *Acoustical aspects of woodwind instruments.* Dekalb: Northern Illinois University Press, rev. ed., 1998.

[33] W. M. Hartmann, *Principles of musical acoustics.* New York, NY: Springer, 2013.

[34] D. H. Keefe, "Wind instrument reflection function measurements in the time domain," *The Journal of the Acoustical Society of America*, vol. 99, no. 4, pp. 2370–2381, 1996.

[35] P. R. Cook, *Introduction to Physical Modeling*, vol. 1, pp. 179–198. Taylor & Francis Group, 2004.

[36] J. O. Smith, "Physical modeling synthesis update," *Computer Music Journal*, vol. 20, no. 2, pp. 44–56, 1996.

[37] U. Zolzer, *DAFX: digital audio effects.* Wiley, 2011.

[38] H. Levine and J. Schwinger, "On the radiation of sound from an unflanged circular pipe," *Physical Review*, vol. 73, no. 4, p. 383, 1948.

[39] C. de Transfert de Technologie du Mans, *Capteur d'Impédance: Manuel D'utilisation.* 2008.

[40] A. Lefevbre and G. Scavone, "A comparison of saxophone impedances and their playing behavior," in *Proceedings of the Forum Acusticum Conference*, (Aalborg, Denmark), pp. 539–544, 2011.

[41] J. C. Le Roux, J.-P. Dalmont, and B. Gazengel, "A new impedance tube for large frequency band measurement of absorbing materials," *Journal of the Acoustical Society of America*, vol. 123, no. 5, p. 3119, 2008.

[42] J.-C. Le Roux, M. Pachebat, and J.-P. Dalmont, "Un capteur de nouvelle génération pour la mesure d'impédance acoustique en contexte industriel," *Acoustique & Techniques*, vol. 68, pp. 6–12, 2012.

[43] G. P. Scavone, "Computational acoustic modeling laboratory." http://www.music.mcgill.ca/caml/doku.php.

[44] A. N. Norris and I. C. Sheng, "Acoustic radiation from a circular pipe with an infinite flange," *Journal of Sound and Vibration*, vol. 135, no. 1, pp. 85–93, 1989.

[45] J.-P. Dalmont, C. J. Nederveen, and N. Joly, "Radiation impedance of tubes with different flanges: numerical and experimental investigations," *Journal of Sound and Vibration*, vol. 244, no. 3, pp. 505–534, 2001.

[46] A. D. Pierce, *Acoustics : an introduction to its physical principles and applications.* Cham, Switzerland: Springer, third ed., 2019.

[47] J.-P. Dalmont, C. J. Nederveen, V. Dubos, S. Ollivier, V. Meserette, and E. te Sligte, "Experimental determination of the equivalent circuit of an open side hole: linear and non linear behaviour," *Acta Acustica united with Acustica*, vol. 88, no. 4, pp. 567–575, 2002.

[48] ROLI Limited, "JUCE 5 [Computer software]." https://juce.com/.